DOTTORATO DI RICERCA IN FISICA

XXVII CICLO

Self-propelled particle models for collective animal behaviour

Dott. Edmondo silvestri
Nome e Cognome del dottorando

firma

Prof. Mauro Rovere
Prof.ssa Irene Giardina
Docente guida/Tutor: Prof.

firma

Prof. Roberto Raimondi
Coordinatore: Prof.

firma

Introduction

Collective behaviour in biological systems is a fascinating field. In autumn the skies of Rome are filled with black clouds displaying harmonious figures. An observer is puzzled, it seams to him to see a single conscious body continuously moving and changing shape. What he's looking at is instead a flock of hundreds or thousands birds, single individuals cooperating to defend themselves from predators.

In general we refer to collective behaviour as all those natural phenomena that involve large groups of animals that spontaneously perform coordinated actions. Often this kind of behaviour occurs by means of individual interactions that have a local nature: each individual interacts with a limited number of neighbours.

The study of collective behaviour includes, in its facets, investigating the features of individual behaviour, the advantages and disadvantages of belonging to the group, the information transfer within it, the process of decision-making, locomotion and synchronization. A fundamental condition for emergent behaviour is that each individual interacts with the others at the same level, without leaders nor external elements that act globally on the system.

In my work I collaborated closely with the COBBS group at the Institute for Complex Systems, CNR, whose objective is *"to understand the fundamental mechanisms of collective behaviour in biological systems through a strong interplay between quantitative empirical observations and theories"*.

In the last years the work of the group has focused on the study of two very different examples of collective behaviour: flocks of birds and swarms of midges. In both cases the group performed worldwide-unsurpassed experiments consisting in filming the system with high speed cameras and reconstructing the three-dimensional trajectories of all the individuals in the system (swarm or flock).

In the birds case this was the natural prosecution of the seminal work led by the group within the STARFLAG project (2005-2008). The higher quality of the new data permitted to study not only the *statical* properties of the flocks (i.e. instantaneous positions and velocities), but also dynamical events such as global changes of direction (turns). From the theoretical point of view, relevant successes where achieved in statistical inference and in the understanding of the transmission of information trough the flock.

The study on midges was instead completely novel. Indeed this was the first study of this type about midges swarming in their natural environment. At the beginning it was even unclear if swarms could be considered or not an example of collective behaviour. We demonstrated that midges actually interact with each other, and that they do so in a way that maximizes the collective response of the system.

In this context my work consisted in part in a daily collaboration to solve the technical problems of trajectories reconstruction; I contributed to the development of the image segmentation algorithm, and provided synthetic data used as a ground-truth for the whole tracking procedure.

My main work concerned the development, the implementation, and the study of numerical models of self propelled particles. For many years the lack of reliable experimental data restricted the study of collective behaviour almost only to numerical models. They are usually based on assumptions about the interaction between individuals, that despite being (in the best case) reasonable, remain at the level of speculation.

I developed new models (and in some cases studied existing ones), incorporating the experimental findings and the consequent theoretical understanding of the systems studied. My objective was to verify through numerical simulations the theoretical predictions, and the effectiveness of the models in reproducing the real phenomenon.

My thesis is structured in three chapters:

In chapter 1 I will summarize the historical experimental results of the STARFLAG project, I will describe an original model whose development was started during my master thesis work and improved during my first year of doctoral school. I will examine the role of the definition of the interaction neighbourhood in keeping the flock cohesive.

I will then present a method of statistical inference, the maximum entropy method, its application to the problem of birds, and its validation through numerical simulations.

Finally I will introduce a novel model directly inspired by the maximum entropy theory. It was one of the first models inspired by these results whose definition is directly derived by the experimental results, and that accounts for the speed of motion of the birds.

In chapter 2 I will summarize the more recent experimental results, whose object of interest was the turning events, i.e. the collective turns performed by flocks during aerial display. Performing a turn implies information transfer through the flock, the analysis of the information flow revealed the limits of the existing theories and led to a new one. I will present a model that embodies the theoretical findings and verify the consequent predictions.

In chapter 3 I will present the experimental results relative to the study of midges swarms. Experiments revealed us that midges swarms belong to the category of collective behaviour despite their lack of global order. I will perform a finite size scaling analysis on a simple self propelled particles model, the Vicsek model, to confirm the experimental indication that midges swarms lie near the critical point of an order–disorder phase transition.

Contents

1 Collective behaviour in bird flocks

Fig. 1.1: A flock of starlings at sunset. Rome, EUR 01/11/2012.

In the last decade a collection of experimental result on collective behaviour was obtained in Rome using stereoscopic techniques to capture starling flocks.

European starlings spend their winter in Rome, feeding during the daylight and coming back to several roosting sites in the city at sunset. It is possible, before roosting, to observe (and film) evolutions of flocks in a relatively confined area in the sky.

Two different trifocal stereo-metric set-up [19, 4] (the second with higher frame rate) were used to capture these evolutions during two observation campaigns in the years 2005-2006 and 2010-2012.

From the collected images it was possible to reconstruct the individual three dimensional positions of the birds and their trajectories over time intervals up to 15 seconds.

In this chapter I will first summarize the results of this experimental study and the theoretical framework developed to understand them, and then I will describe the numerical models that I developed and implemented to test the theory and incorporate the experimental findings.

1.1 Experimental findings

1.1.1 Three dimensional structure

The first possible investigation concerns the spatial structure of the flocks: are they ordered and packed like in crystal lattice, as a eye observation would suggest? Or are they randomly distributed in the flock volume?

The analysis of the packing fraction,

$$\Phi = \frac{4}{3}\pi\rho_H^4 < 0.012, \tag{1.1}$$

and the pair correlation function,

$$g(r) = \frac{1}{4\pi r^2}\frac{1}{\tilde{N}}\sum_{i=1}^{\tilde{N}}\sum_{j\neq i}\delta(r - r_{ij}), \tag{1.2}$$

shows that the system is much more similar to a gas than to a crystal (Fig. 1.2)

The packing fraction of equation (1.1) is the ratio between the total exclusion volume of the birds Nr^3 (being r approximately the wing length) and the total volume of the flock (N/ρ). In a crystal its typical value is of order 0.5.

The pair correlation function (1.2) is a measure of the structure of the system. It calculated as the number of pairs of birds at distance r from each other ($\tilde{N}$ is the number of birds considered in the evaluation of $g(r)$ after the correction of border effects, see [15, 18] for details). In a regular lattice it appears as a periodic series of delta functions, in a liquid It is a damped oscillating curve, while in a gas it's a flat curve.

The $g(r)$ displayed in figure 1.2, with very weak peaks, indicates a structure in mutual distances which is almost gas-like.

As we will see, reproducing this apparently uninteresting result in a simulation can be quite challenging.

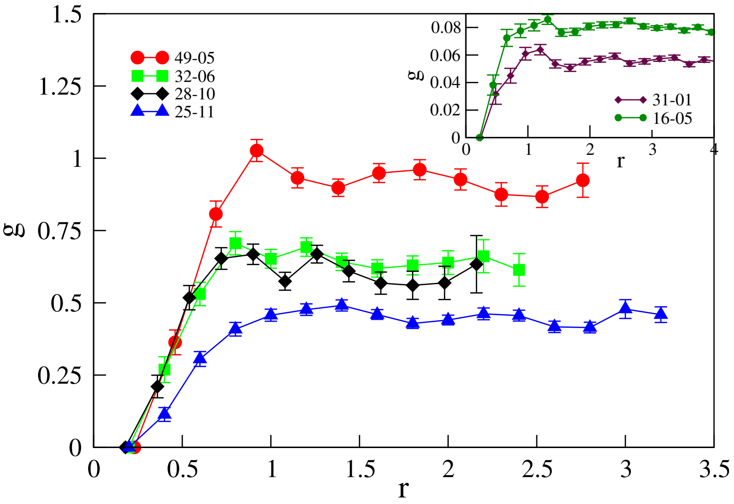

Fig. 1.2: Pair correlation function $g(r)$ of some flocks. Each curve corresponds to a flock at a single instant of time. Flocks with low density are shown in the Inset. In a lattice structure it would appear as a periodic series of delta functions, while in a liquid structure as a damped oscillating curve and in a gas it would be flat. The weak peaks indicate an almost gas-like structure. Figure from [15].

1.1.2 Topological interaction

Even tough the $g(r)$ is gas-like, flocks have a non trivial spatial structure. This can be seen by looking at angular distributions and taking into account the mean direction of motion. For example if we look at the distribution of the first nearest neighbour we find it clearly anisotropic; the probability of finding the nearest neighbour in the direction of the wings is significantly higher than in the direction of motion. The distribution of the tenth neighbour instead is uniform in the solid angle, indicating that the anisotropy decays with the order of neighbourhood [7].

This anisotropy gives a hint about the interaction range of the birds. If the anisotropy is a consequence of interaction, then when it vanishes there should be no more interaction.

To have a more precise measure of anisotropy decay, we define the anisotropy factor $\gamma(n)$ that measure the probability to find the n^{th} neighbour along the direction of motion; it is defined as the squared scalar product of the normalized vectors $\hat{\boldsymbol{v}}$ and $\hat{\boldsymbol{w}}$,

$$\gamma = (\hat{\boldsymbol{v}} \cdot \hat{\boldsymbol{w}})^2 \qquad \gamma \in [0,1] \tag{1.3}$$

where $\hat{\boldsymbol{v}}$ is the mean direction of motion, and $\hat{\boldsymbol{w}}$ is the direction of minimal crowding of the n^{th} nearest neighbour. $\hat{\boldsymbol{w}}$ can be calculated as the eigenvector relative to the lowest eigenvalue of the matrix M with elements:

$$\sum_{\beta} \boldsymbol{M}_{\alpha\beta} v_\beta = u^i_\alpha \sum_{\beta} u^i_\beta v_\beta \qquad \alpha, \beta = x, y, z \tag{1.4}$$

whose components $\hat{\boldsymbol{u}}_i$ are the normalized position of the n^{th} nearest neighbour of i relative to the position of i, $\boldsymbol{u}_i = ((r)_{th} - \boldsymbol{r}_i)/|(r)_{th} - \boldsymbol{r}_i|$. The value of $\gamma(n)$ for a isotropic distribution is 1/3 while in the case of birds it is significantly higher than 1/3 for $n \lesssim 7$ as shown in (Fig. 1.3a).

The value of n_c for which $\gamma(n)$ decays to 1/3 is a proxy of the interaction range.

Surprisingly this n_c is constant for flocks of different densities or, in other terms it doesn't depend by the distance of neighbours. This was the first evidence of a topological interaction: every birds interacts with a fixed and small ($n_c \sim 7$) number of neighbours, independently of their distance. The idea of topological interaction have a very reasonable efficiency meaning: if the range of interaction is not dependent from the distance, then the probability to maintain cohesion is enhanced (see section 1.2.3).

1.1.3 Velocity correlation functions

Flocks of birds appear to be very ordered even just to the naked eye observation, the birds fly all in the same direction. In fact if we evaluate the

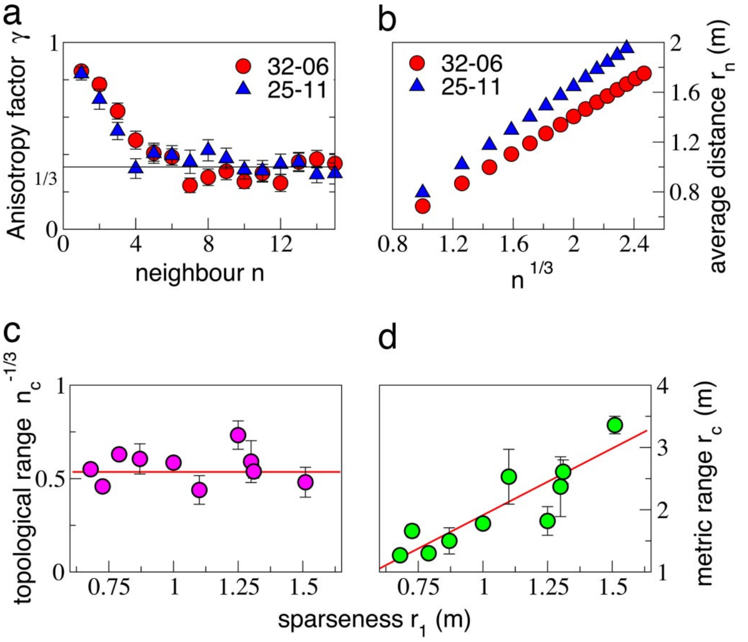

Fig. 1.3: **(a)** the function $\gamma(n)$ measures the anisotropy of the angular distribution with respect to the direction of motion. $\gamma(n)$ is defined between 0 and 1. A value of $\gamma(n)$ close to 1 indicates that there is a very low probability to find the n^{th} nearest neighbour along the direction of motion (i.e. there is a strong anisotropy). The value 1/3 corresponds to an isotropic distribution of neighbours. The topological range n_c is defined as the value of n for which the function $\gamma(n)$ reaches the value 1/3. **(b)** average distance of the n^{th} neighbour. **(c)** The topological range of interaction is uncorrelated with the distance of the first neighbour (inverse of the density) while the metric range **(c)** is. This is clearly indicating that the interaction is based on the topological range. Figure from [7].

polarization of a flock as:

$$\Phi = \frac{1}{N} \left| \sum_{i=1}^{N} \frac{\boldsymbol{v}_i}{|\boldsymbol{v}_i|} \right| , \tag{1.5}$$

we find $\Phi \sim 0.98$. It seems very reasonable (quite obvious) that this high alignment is a consequence of the interaction, but in principle this can happen also for other reason, for example there can be an external force or the flock can be driven by a leader.

The most reliable sign of a local interaction comes from the connected correlation function [10]:

$$C(r) = \frac{\sum_{ij} \boldsymbol{u}_i \cdot \boldsymbol{u}_j \delta(r - r_{ij})}{\sum_{ij} \delta(r - r_{ij})}, \tag{1.6}$$

with $\boldsymbol{u}_i$ being the i^{th}s bird velocity in the flock's centre of mass reference frame.

$$\boldsymbol{u}_i = \boldsymbol{v}_i - \frac{1}{N} \sum_{k=1}^{N} \boldsymbol{v}_k \tag{1.7}$$

Equation (1.6) measures how much the fluctuations of the velocities of two birds at distance r are correlated.

It's important to use the connected correlation function and take care of all possible global motions because we want to measure only correlation that are consequence of social interaction. If we instead omit to subtract the mean motion in the correlation function e.g. calculating the non connected one:

$$C(r)_{nonconnected} = \frac{\sum_{ij} \boldsymbol{v}_i \cdot \boldsymbol{v}_j \delta(r - r_{ij})}{\sum_{ij} \delta(r - r_{ij})}, \tag{1.8}$$

we will obtain something that is clearly dominated by the mean velocity, and we can get high correlation even without interaction (for example due to external forces or leaders).

Equation (1.6) is the correlation of the full vectorial velocities, and it's importance is very clear when we think that alignment is the most evident consequence of interaction, but it's also possible, and indeed interesting, to evaluate the correlation of speed:

$$C_{sp}(r) = \frac{\sum_{ij} \varphi_i \cdot \varphi_j \delta(r - r_{ij})}{\sum_{ij} \delta(r - r_{ij})} \tag{1.9}$$

where φ_i is the fluctuation of the speed (the modulus of $\boldsymbol{v}$).

$$\varphi_i = |\boldsymbol{v}_i| - \frac{1}{N}\sum_{k=1}^{N} |\boldsymbol{v}_k| \,.$$

In figure 1.4a and 1.4b are shown the correlation function for orientation and speed respectively. The correlation functions defined in equations (1.6) and (1.9) have to cross the zero at least once because the integral of their numerator is zero by construction; the value of $\xi = r_0$ with $C(r_0) = 0$ is proportional to the correlation length of the system [16]. Looking at figure 1.4c and 1.4d we find that the correlation lengths grow linearly with the distance. Both correlation of speed and orientation are therefore scale free.

The correlation length is a measure of the capability of a system to respond to external stimuli. In physical systems the correlation is proportional to the response exhibited by the system to perturbations. Scale free correlation therefore indicate that flocks respond collectively.

Scale free correlations can be expected for the orientations (it is possible to prove that fluctuations transverse to the order parameter are scale free see: Goldstone's theorem [1], and SI in [8] for details), they are harder to explain in the case of speed. The optimal speed of flight is reasonably determined by physical constrains, flying too fast will result in an excessive energy consumption, while flying too slow would mean to fall on the ground. But if the optimal speed was only determined by the flying physics, one could expect uncorrelated speed fluctuations, that are instead strongly correlated.

In statistical physics scale free correlations are often associated with criticality. Evidences of criticality have been examined in biological systems as diverse as bird flocks, neural networks and amino-acid chains [31], and also, as we will see in chapter 3, midge swarms. The idea that criticality could be a general features in biological systems is currently discussed by the scientific community, it is however reasonable to think that being near the critical point of a phase transition is advantageous. Being critical maximizes the collective response to perturbations.

1.1.4 Summary of experimental results

Experiments revealed us some important properties of bird flocks that need to be theoretically understood.

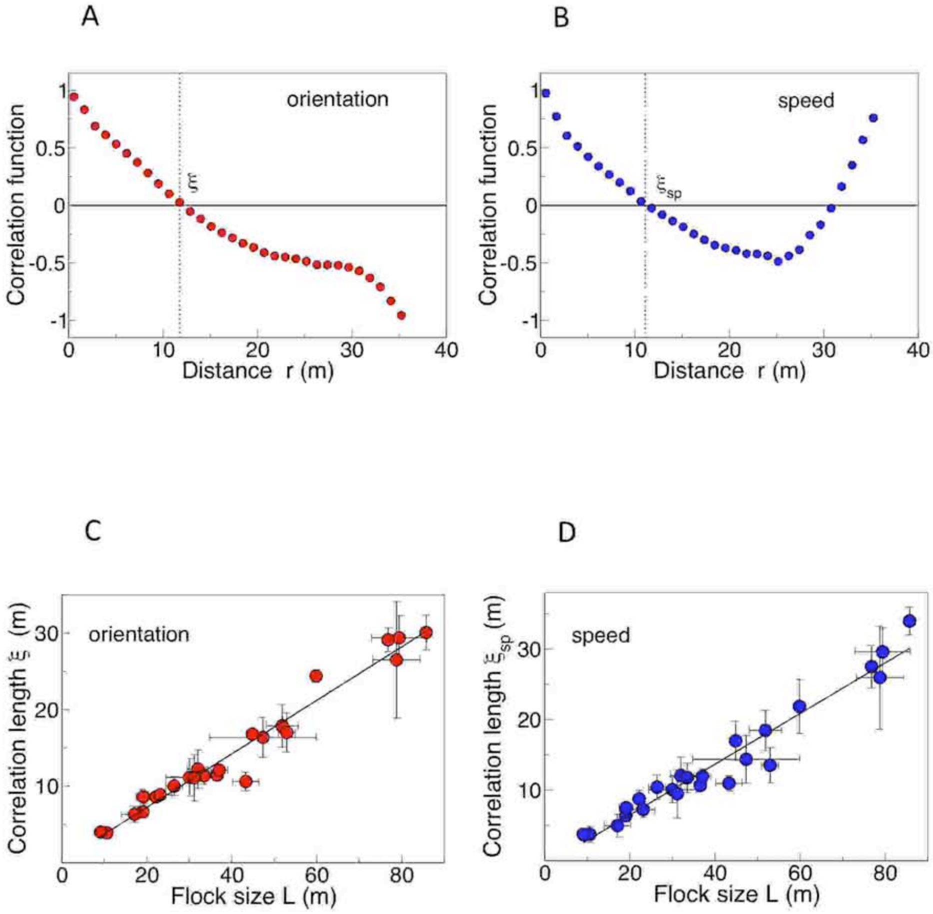

Fig. 1.4: **a** and **b** correlation function of direction and speed respectively. The first crossing of the x axis gives an estimate of the correlation length, that is showed in the lower panels in function of different flock sizes, where we find a clear linear dependence with no sign of saturation. The correlation length are therefore scale-free. Figure from [16].

The three dimensional structure is much similar to a gaseous system than to a crystalline one. Flocks are however not completely unstructured, they are anisotropic with respect to the direction of motion; this revealed a fundamental characteristic of their interaction: it is topological and not metric. Is the topological interaction the key feature in keeping efficiently the cohesion of the flock?

Flocks are strongly ordered, with scale free correlation of the fluctuations of both orientation and speed. The correlation length is of order of the system size. This implies a high degree of mutual influence even tough the interaction is short range ($6 \sim 7$ neighbours).

In the next section I will summarize the theoretical explanations of these results and I will address the attention to the comparison between existing and novel models with the experimental and theoretical results.

1.2 Numerical models of flocking

1.2.1 The Vicsek model

The Vicsek model [46] is the archetype of almost all flocking models. It consists in a system of particles moving of lattice and updating their state, defined by a position $\boldsymbol{r}$ and a direction $\boldsymbol{v}$, via a simple interaction rule.

The Vicsek model is based upon three reasonable assumptions: **i)** since the birds are strongly aligned, then each bird i has to adjust its direction evaluating the mean direction of the others (alignment interaction); **ii)** a bird will not be able to follow all the others, but only the neighbours within a certain radius (short range interaction); **iii)** the bird's motion will be subject to some sort of noise due to environment perturbation or cognitive errors.

In its original formulation each particle tends to align its direction of motion to that of its metric neighbours. More precisely, the direction of particle i at time $t + 1$ is the average direction of all particles within a sphere of radius λ around i (including i itself). The parameter λ is therefore the metric radius of interaction, that is the perception range. The resulting direction of motion is then perturbed with a random rotation, playing the role of noise. Particles have all fixed velocity modulus $|\boldsymbol{v}| = v_0$. The update equation of the model is,

$$\boldsymbol{v}_i(t+1) = v_0 \; \mathcal{R}_\eta \left[\Theta \left(\sum_{j \in S_i} \boldsymbol{v}_j(t) \right) \right] , \tag{1.10}$$

where S_i is the spherical neighbourhood of radius λ centred around i, Θ is the normalization operator $\Theta(\boldsymbol{x}) = \boldsymbol{x}/|\boldsymbol{x}|$ and $\mathcal{R}_\eta$ performs a random rotation uniformly distributed around the argument vector with a maximum amplitude of $4\pi\eta$. The position r_i is updated with the following rule,

$$\boldsymbol{r}_i(t+1) = \boldsymbol{r}_i(t) + \boldsymbol{v}_i(t+1). \tag{1.11}$$

When the interaction radius λ is fixed (typically set equal to one) the behaviour of the model is independent from the value of v_0 if it is below a given threshold ($v_0 \lesssim 0.5$) meaning that in order to align with the others, a particle should not change its neighbourhood too quickly. The remaining independent parameters, the density ρ and the noise η, completely determine the behaviour of the system. The density is implicitly set by the number of particles and by the size of the box (usually with periodic boundary conditions) where the system evolves.

The most widely studied property of the Vicsek model is its order-disorder transition. This transition is driven either from the noise amplitude or from the density of the system. When the noise (density) is above (below) a critical value the system is disordered, while it is ordered vice versa. The critical value of one parameter depends by the (fixed) other. In the limit of zero density (open boundary conditions) there is no ordering.

The nature of this transition has been long debated [46, 21, 24, 25, 20], and finally proved to be first order. However the phenomenology is indistinguishable from a second order transition up to very large system sizes.

In a first order transition the correlation length is generally finite even at the critical point, nevertheless, if it is very large, it is possible to observe scale free correlation up to large scales, exactly as if the transition was second order [10].

A quantity that clearly displays the difference between continuous and discontinuous transition is the Binder cumulant,

$$G(\eta, L) = 1 - \frac{\langle \phi^4 \rangle_t}{3 \langle \phi^2 \rangle_t^2}, \tag{1.12}$$

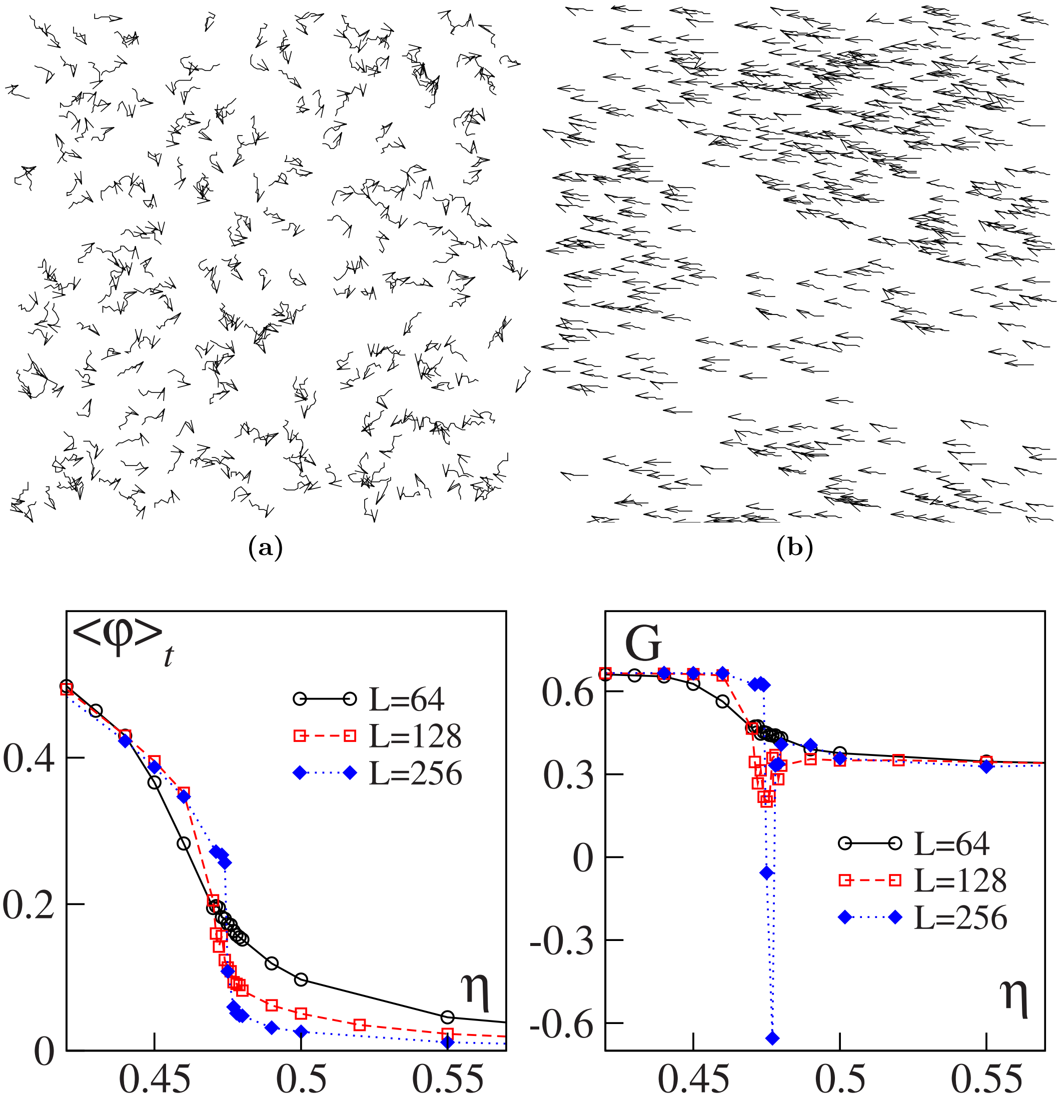

Fig. 1.5: (a) and (b) snapshots of the Vicsek behaviour in the disordered and ordered phases. Figure from [46]. (c) Behaviour of the polarization with respect to noise at fixed density ($\rho = 2$). The critical point is at $\eta \sim 0.46$. (d) Binder cumulant, a clear drop toward negative values is evident for large system sizes, indicating the discontinuous nature of the transition. Figure from [20].

where ϕ is the instantaneous polarization and $\langle\cdot\rangle_t$ denotes the time average. The Binder cumulant is $G(\eta, L) \sim 2/3$ in the ordered phase, while in the disordered one it is $G(\eta, L) \sim 1/3$ in 2d ans $G(\eta, L) \sim 4/9$ in 3d. If the phase transition is second order the Binder cumulant has an universal value at the critical point, so that for different system sizes L the curves $G(\eta, L)$ cross each others in the same point. On the other hand if the transition is first order $G(\eta, L)$ has a sharp drop toward negative values at the critical point, as a consequence of the coexistence of the two phases (Fig. 1.5d).

There are indeed two immediately evident aspects of this model that deeply differ from the real flocks of birds: the model has no attraction repulsion interaction and it will evaporate (as a gas) in free boundary conditions, and more importantly the interaction range is metric.

1.2.2 The Grègoire, Chatè and Tu model

An important modification of the Vicsek model was carried on by Grègoire, Chatè and Tu in [26, 25]. They focused their attention on the cohesion of the flock.

The cohesion of the flock in free boundary conditions is guaranteed (with the right set of parameters) by an additional attraction repulsion term, that as for Vicsek is based upon some reasonable assumption: a bird will try to avoid collisions, and to maintain a fixed distance from the others.

The interaction rule is defined imposing that the interaction ensemble of each particle is given by the links drawn building the Delaunay triangulation of the points corresponding to the particles positions. The Delaunay triangulation is the geometrical triangulation that maximize the internal angles of the triangles (in 2d) or the simplexes (in arbitrary dimension). In two dimensions, given a collection of points in the plane, a triangulation consists in drawing triangles using all the points as vertices; such triangulation is a valid Delaunay triangulation if the circumscribed circle of each triangle does not contain points other than the triangle vertices [34]. Additionally a metric cut-off of the interaction is imposed to avoid the possibility of long range interaction. Thus, this is a mixed metric-topological rule.

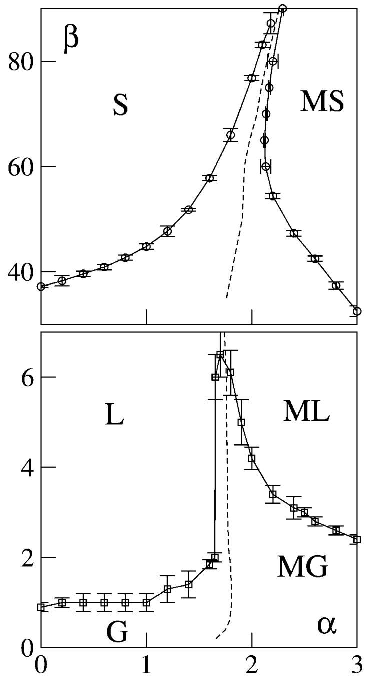

Fig. 1.6: Phase diagram of the Grègoire and Chatè model in the $\alpha - \beta$ plane (i.e. at fixed noise and density). The two panels represent two regions far from each other on the β axis. There are two horizontal separation between the gaseous G and the liquid L phases and between the liquid and solid S ones depending by the parameter β, and a vertical separation between the moving an non moving phases depending from α. The transition between moving and not moving is analogous to the order/disorder transition in the standard Vicsek model (where it is the only possible transition), and it is mainly driven by the ratio between alignment and noise; the gas–liquid–solid transitions are determined by the attraction repulsion strength: when it is high the particles naturally arrange themselves in a lattice–like distribution as a system of packed spheres would do, while if the attraction force is low the system will evaporate. The parameters are: $\rho = 1/16$, $L = 180$, $v_0 = 0.05$, $\eta = 1.0$, $r_c = 0.2$, $r_e = 0.5$, $r_a = 0.8$ and $r_0 = 1.0$. Figure from [26].

The Vicsek model is thus modified as follows,

$$\boldsymbol{v}_i(t+1) = v_0 \Theta \left[\alpha \sum_{j \in D_i} \boldsymbol{v}_j(t) + \beta \sum_{j \in D_i} \boldsymbol{f}_{ij} + n_c \boldsymbol{\eta}_i \right] \tag{1.13}$$

$$\boldsymbol{x}_i(t+1) = \boldsymbol{x}_i(t) + \boldsymbol{v}_i(t), , \tag{1.14}$$

where D_i is the set of Delaunay neighbours of particle i, n_c the number of particles in D_i (i.e. the number of i's interacting neighbours) and f_{ij} is an attraction repulsion term in the form,

$$\boldsymbol{f}_{ij} = \hat{\boldsymbol{r}}_{ij} \begin{cases} -\infty & \text{if } r_{ij} < r_c \\ \frac{1}{4}\frac{r_{ij}-r_e}{r_a-r_c} & \text{if } r_c < r_{ij} < r_a \\ 1 & \text{if } r_a < r_{ij} < r_0 \end{cases} , \tag{1.15}$$

here r_c is a hard sphere repulsion distance, r_e is the equilibrium of the elastic potential, r_a a threshold distance beyond which the attraction force becomes constant, and r_0 the maximum interaction range. Typical values for these parameters are $r_c = 0.2$, $r_e = 0.5$ and $r_a = 0.8$, in order to have a balanced proportion between attraction and repulsion zones when $r_0 = 1$. The precise form of the dependence of this attraction repulsion term has to be non crucial. The underlying idea is to have an hard core repulsion term, an equilibrium distance, and a threshold on the maximum force that should not grow indefinitely with distance.

The noise term was also redefined, introducing what was called *vectorial* noise that, in contrast with the *angular* noise defined by Vicsek, it is dependent from the number of interacting neighbours to mimic the error made by a bird following one other.

This model has a richer phase diagram with respect to the Vicsek's one. In the $\alpha - \beta$ plane (i.e. fixed density and noise) we can observe horizontal transition lines between the gas/liquid and liquid/solid phases and a vertical transition between the not-moving/moving ones. (Fig. 1.6).

1.2.3 The topological Vicsek model

The Grègoire, Chatè model is a first step in the investigation of the role of topological interaction in flocking, but to understand if topological interaction enhances the efficiency of the system we need something different.

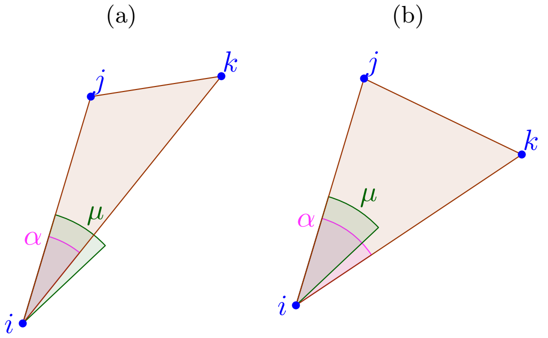

Fig. 1.7: Topological model with angular resolution. The interaction ensemble $\mathrm{S}(i)$ is defined in the following way. Let j and k be the first and second nearest neighbours of particle i ($r_{ij} < r_{ik}$, $r_{ij} = |\boldsymbol{r}_{ij}|$, $r_{ik} = |\boldsymbol{r}_{ik}|$). If we call μ a threshold parameter and α the angle $\widehat{jik}$, then i interacts only with j if $\alpha < \mu$ **(a)**, while it interacts with j *and* k if $\alpha > \mu$ **(b)**. This rule is iteratively applied to all the pairs of neighbours of i, choosing the nearest one every time that the angle between the particles is smaller than the threshold. The value of μ also fixes the average number of interacting neighbours $n_c(\mu) = (1/N)\sum_i n_c^i$. One can show that approximately $n_c(\mu) \sim 2/(1-\cos(\mu))$. Figure from [13].

In [7] was proposed a first comparison between a metric and topological model, showing that in the topological case the probability to maintain the cohesion is higher. Here I'll present a further investigation in this direction.

The simplest possible definition of topological interaction consists in imposing that each bird interacts only with the first n_c nearest neighbours. In this case there is indeed the possibility for a bird to be subject to a directionally unbalanced transfer of information. If a bird's neighbours are all on one side except one on the other, the information coming from the isolated bird will have an insignificant weight with respect to the information coming from the many *same-side* others which will be indeed redundant.

I added to the simple topological rule an assumption: a bird will try to gather information from all directions, neglecting redundancy to optimize its cognitive capabilities.

I therefore defined [13] an interaction rule based on a threshold on the angular distance between the neighbours of each bird: if two neighbours are (angularly) too near to each other, a bird will interact only with one of them, the nearest. A clear graphical explanation is given in figure 1.7.

To investigate the cohesion performance of metric and topological interaction I used three variants of the model defined by the update rules of equations (1.13) and (1.11), where the ensemble of interacting neighbours of each bird is defined by a metric rule, by the simple topological rule and finally by the last defined *balanced* topological rule. The model is thus redefined as,

$$\boldsymbol{v}_i(t+1) = v_0 \Theta \left[\alpha \sum_{j \in S_i} \boldsymbol{v}_j(t) + \beta \sum_{j \in S_i} \boldsymbol{f}_{ij} + n_c \boldsymbol{\eta}_i \right] \tag{1.16}$$

$$\boldsymbol{x}_i(t+1) = \boldsymbol{x}_i(t) + \boldsymbol{v}_i(t), \tag{1.17}$$

Where S_i is the interaction ensemble defined either with the metric, simple topological or balanced rule. $\boldsymbol{f}_{ij}$ has the same definition as the Grègoire, Chatè model, with the value of r_0 equal to infinity in the two topological variants.

$$\boldsymbol{f}_{ij} = \hat{\boldsymbol{r}}_{ij} \begin{cases} -\infty & \text{if } r_{ij} < r_c \\ \frac{1}{4} \frac{r_{ij} - r_e}{r_a - r_c} & \text{if } r_c < r_{ij} < r_a \\ 1 & \text{if } r_a < r_{ij} < r_0 \end{cases} \tag{1.18}$$

Here is important to stress that the topological nature of the interaction is relative to the rule used to determine the interaction ensemble of each particle, and using a metric equilibrium distance doesn't infringe this nature.

I compared [13] the behaviour of these three variants against noise and against an external perturbation. This comparison consisted in simulating the evolution of the system during a fixed time interval (with the appropriate set of parameters) and counting the number of connected components (CC) formed by the (eventual) splitting of the initially cohesive flock. A large number of CC implies low stability, and vice-versa. Each experiment was repeated 400 times and averages were performed over all these runs.

When comparing the resilience of different models to noise, η, one must of course use the same value of η in all three models, otherwise the comparison would be unfair. In this case, thus, one must use the same value also for all parameters other than noise. Concerning the range, this means fixing r_0 and μ such that the effective number of interacting neighbours, n_c, is the same in all three models. This 'equal parameters' comparison is a neutral (and natural) path to be investigated.

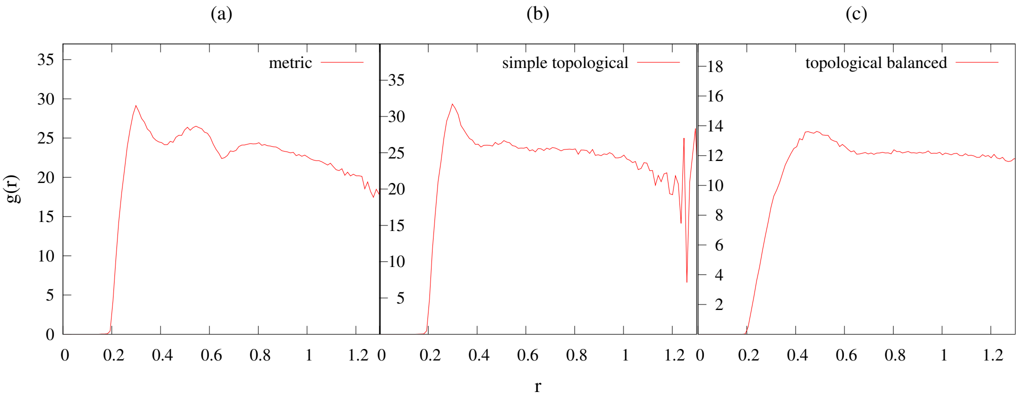

Fig. 1.8: $g(r)$ function for the three models at equal observables. For all three models, observables are polarization $\Phi = 0.99$ and number of connected components $< CC >= 1$. Fixing the observable means tuning the parameters individually for each model.
(a) Metric model: $\alpha = 35$, $\beta = 0.5$, $\eta = 0.25$, $r_c = 0.65$ (implying $n_c(r_0) = 21.2$).
(b) Purely topological model: $\alpha = 35$, $\beta = 0.25$, $\eta = 0.25$, $n_c = 20$.
(c) Topologically balanced model: $\alpha = 35$, $\beta = 0.06$, $\eta = 0.125$, $\mu = 0.7$ (implying $n_c(\mu) = 8.8$).
Figure from [13].

However, using equal parameters is not the right thing to do when one wants to test the stability against external perturbations. The three models are different, and therefore same values of the parameters may imply different biological observables. Hence, the second criterion I adopted was to use for each model a different set of parameters (a sort of optimal set) (Fig. 1.8) that ensures a realistic value of polarization and cohesion, and as realistic as possible a radial correlation function, $g(r)$. Once this calibration to the biological observables is done, it's possible to proceed with the comparison of the model's performance against external perturbation.

A summary of the results is presented in figure 1.9 where the probability distribution of CC is showed against noise (Fig. 1.9a) and obstacle (Fig. 1.9b).

My analysis confirms that topological interaction perform better than metric one. The problem with metric interaction is that individuals can easily drop out of the interaction range, hence losing contact with the rest of the

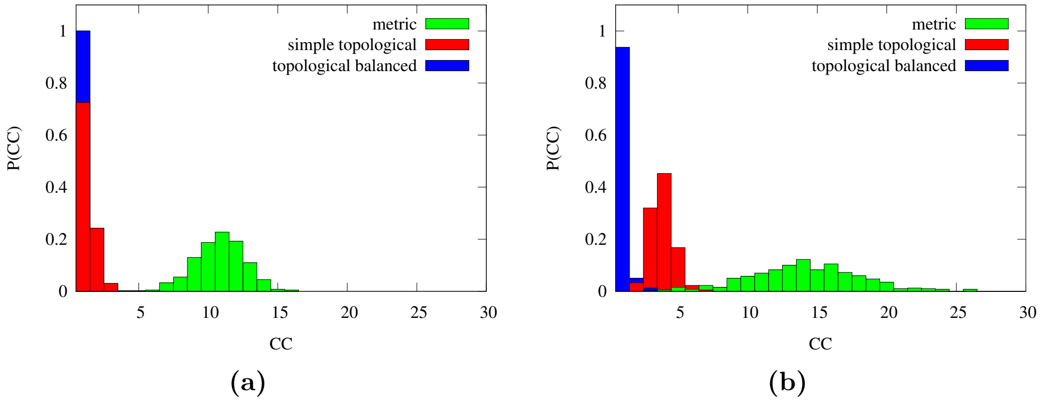

(a) **(b)**

Fig. 1.9: (a) Probability that a flock splits into M connected components after 5000 iterations, for the three variants of the model (metric, green bars; simple topological, red bars; and topological balanced, blue bars). An initially cohesive flock is left to evolve unperturbed according to equations 1.16 and 1.17. Owing to the presence of noise, the flock can spontaneously split giving rise to multiple sub-groups. $n_c = 22$ for the simple topological model; $r_0 = 0.72$ for the metric model (corresponding to $n_c(r_c) \sim 22$); and $\mu = 0.411$ for the topological balanced model (corresponding to $n_c(\mu) \sim 22$). $N = 512$, $\alpha = 35$, $\beta = 5$, $\eta = 1$. The other parameters are ($v_0 = 0.05$, $r_c = 0.2$, $r_e = 0.5$, $r_a = 0.8$). 400 distinct simulation runs are performed for each histogram. (b) same as (a), but with the system perturbed by an obstacle. The obstacle is placed in the direction of motion of the flock (in axis with its centre of mass) approximately at a distance of twice the flock radius. The obstacle is modelled as a sphere of radius 2. When a bird's distance from the obstacle is smaller than the sphere radius, it takes the opposite direction with respect to the obstacle, regardless of its neighbours. Metric model: $\alpha = 35$, $\beta = 0.5$, $\eta = 0.25$, $r_0 = 0.65$ (implying $n_c(r_0) = 21.2$). simple topological model: $\alpha = 35$, $\beta = 0.25$, $\eta = 0.25$, $n_c = 20$. Topologically balanced model: $\alpha = 35$, $\beta = 0.06$, $\eta = 0.125$, $\mu = 0.7$ (implying $n_c(\mu) = 8.8$). Figure from [13].

group. However, even the purely topological model is unstable with respect to fragmentation into sub-groups of size n_c. The only way to respond to such instabilities, for both metric and purely topological model, is to increase the number of interacting neighbours, which may lead to flocks that are cohesive but with too strong a structure compared to real ones. The radial correlation function, which has been measured in real flocks, is the main tool I used to check particles' positional structure within the flock.

In figure 1.8 I show the $g(r)$ obtained from the simulation of the three models using the *optimal* set of parameters. In the metric and simple topological cases the density (ideally the limit $g(r \to \infty)$) is higher and the peaks of the $g(r)$ are still more pronounced than in the balanced case.

On the other hand, I found that using a topological rule that is balanced in space, where neighbours are selected topologically, but at the same time they are evenly distributed in angle, it is possible to achieve robust cohesion also with a small number of interacting neighbours, still preserving a realistic structure for the flock, namely a realistic $g(r)$. When I fix parameters independently in each model in such a way that all three models have realistic polarization and structure, and high unperturbed cohesion, it turns out that the topologically balanced mode has the highest stability against external perturbation (Fig. 1.9).

Model implementation

To conclude this section I add a brief comment on the model implementation. The standard implementation of the Vicsek model (valid in general for numerical simulations of particle systems with short range metric interactions) consists in partitioning the space in a (usually) uniform grid. If the cell size of the grid is chosen equal to the interaction radius, then to compute the interactions for a given particle i is sufficient to explore the cell containing i and the surrounding ones and compute the interaction with the particles j contained in those cells.

This algorithm is intrinsically not suitable in the case of topological interactions since there is no metric limit to the maximum distance of interaction between two particles. An alternative (indeed used for k-nearest-neighbour search [23]) is to compute the all pair distances, for each particle sort them by distance, and use the first n_c to compute the interactions. Obviously this alternative has a high computational complexity ($O(N^2)$) and can be reasonably

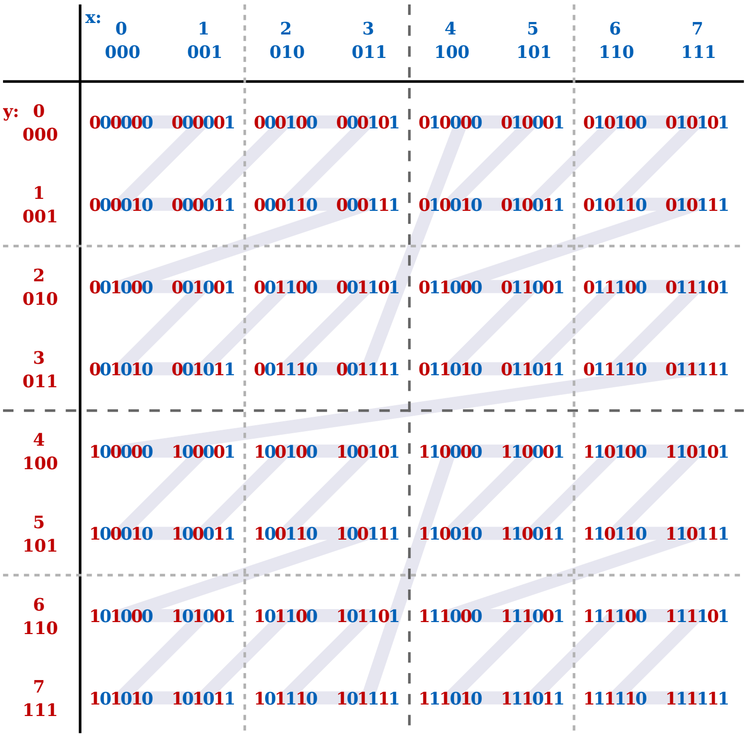

	x: 0 000	1 001	2 010	3 011	4 100	5 101	6 110	7 111
y: 0 000	000000	000001	000100	000101	010000	010001	010100	010101
1 001	000010	000011	000110	000111	010010	010011	010110	010111
2 010	001000	001001	001100	001101	011000	011001	011100	011101
3 011	001010	001011	001110	001111	011010	011011	011110	011111
4 100	100000	100001	100100	100101	110000	110001	110100	110101
5 101	100010	100011	100110	100111	110010	110011	110110	110111
6 110	101000	101001	101100	101101	111000	111001	111100	111101
7 111	101010	101011	101110	101111	111010	111011	111110	111111

Fig. 1.10: Graphical representation of the two dimensional Z-order space partitioning. A cell's index consists in a binary number whose even bits are the x coordinate of the cell and odd ones are the y coordinate.

used only for small Ns.

I instead implemented a Z-order space partitioning [33]. It consists in defining a particle's cell index interleaving the bits of the cell's coordinates (Fig. 1.10). For example, in 2d, a cell of coordinates (6,5) has in binary representation coordinates (110,101); its index in the Z-order is 110110 $= 54$. The Z-curve has scaling self-similarity (its pattern is repeated at different scales), so cells are automatically arranged in levels of a tree structure; if one need to know the index of a higher level is sufficient to shift the lowest level's index by two bits on the right; in the previous example it would be 110110 $>> 2 =$ 1101 $= 13$ (where $>>$ is the bit shift operator).

If now the particles are indexed by their cell coordinates following the z-curve, and they are sorted by this index (at each simulation iteration), then all the particles belonging to the same cell are contiguous in the ordered list, and this is true for all the levels of the tree structure composed by cells and sub-cells of arbitrary depth. This means that to iterate over the particles in a cell it is sufficient to know the indexes of the first and last ones in that cell.

During the simulation, the distance of the furthest interacting neighbour is known for each particle from the previous simulation step, and since the speed is fixed this distance can not increment more than twice the speed (with the two particles going in opposite directions). Accordingly it is known the level of the cells tree that has a cell size greater or equal to the furthest interacting neighbour's maximum distance; the new interacting neighbours will be searched exploring this level's cell.

All the models I will present in this thesis are based on this algorithm whose merit is also the flexibility: it works well also for the metric interactions.

To my knowledge this algorithm implementation for topological interaction in self propelled particles is original, while the use of z-ordering to solve the so called *k-nearest-neighbour* search problem was first described in a database optimization work [37].

I implemented this algorithm on GPU using the CUDA C programming language, taking advantage not only from the high GPU computing performance (a deep performance analysis was out of my scope), but also from the possibility to have a graphical representation of the evolving system in real time on the monitor. Some of my results originate from initial intuitions I had just looking at coloured particles moving on my monitor during real time simulations.

1.3 The maximum entropy approach and a model for speed fluctuations

The models presented in the previous section are based on assumptions (e.g take the average direction of neighbours), these are reasonable but still arbitrary ones.

In this section I will briefly introduce a theoretical statistical inference method; I will describe how it can be applied to flocking experimental data, and validate the method against numerical simulations; finally I will introduce a novel self-propelled particle model whose interaction rules are inspired by the theory rather than assumptions.

1.3.1 Maximum entropy theory for the flight directions

The maximum entropy theory [28] provide us an analytical method to infer the probability distribution of an observable using the experimental measures with the minimum (ideally null) number of assumptions.

Given an observable $\boldsymbol{u}_i$, we can think that it is drawn from a probability distribution $P(\{\boldsymbol{u}_i\})$. The maximum entropy method consists in finding the less structured (most random) distribution P among the infinite possible ones.

From Shannon's information theory [40] we know that the measure of randomness (or the measure of information) is given by entropy:

$$S[P] = -\sum_{\boldsymbol{u}} P(\boldsymbol{u}) \ln P(\boldsymbol{u}). \tag{1.19}$$

We wan to to maximize $S[P]$ subject to the constraint that the expectation values computed with P match the experimental measures,

$$\langle f_\mu(\boldsymbol{u}) \rangle_{exp} = \langle f_\mu(\boldsymbol{u}) \rangle_P \equiv \sum_{\boldsymbol{u}} P(\boldsymbol{u}) f_\mu(\boldsymbol{u}) \qquad \forall \mu, \tag{1.20}$$

with the additional constraint that $P(\boldsymbol{u})$ should be normalized, $f_0(\boldsymbol{u}) = 1$. We can use the method of Lagrange multipliers to solve this optimization problem introducing a generalized entropy function,

$$\mathcal{S}[P;\lambda_\nu] = S[P] - \sum_{\mu=0}^{K} \lambda_\mu \left[\langle f_\mu(\boldsymbol{u}) \rangle_P - \langle f_\mu(\boldsymbol{u}) \rangle_{exp} \right], \tag{1.21}$$

where a multiplier λ_μ is added for each constraint. Maximizing $\mathcal{S}$ with respect to P we obtain:

$$\begin{aligned} 0 &= \frac{\partial \mathcal{S}}{\partial P} \\ &= \frac{\partial S}{\partial P} - \sum_{\mu=0}^{K} \frac{\partial \langle f_\mu(\boldsymbol{u}) \rangle_P}{\partial P} \\ &= -\ln P(\boldsymbol{u}) - 1 - \sum_{\mu=0}^{K} \lambda_\mu f_\mu(\boldsymbol{u}) \qquad (1.22) \\ \Rightarrow P(\boldsymbol{u}) &= \frac{1}{Z(\{\lambda_\nu\})} \exp\left[-\sum_{\mu=0}^{K} \lambda_\mu f_\mu(\boldsymbol{u}) \right], \qquad (1.23) \end{aligned}$$

with,

$$Z(\{\lambda_\nu\}) = \sum_{\boldsymbol{u}} \exp\left[-\sum_{\mu=0}^{K} \lambda_\mu f_\mu(\boldsymbol{u})\right]. \tag{1.24}$$

Optimizing with respect to $\{\lambda_\nu\}$ we obtain a set of K simultaneous equations

$$\begin{aligned} 0 &= \frac{\partial \mathcal{S}}{\partial \lambda_\mu} \\ &= \langle f_\mu(\boldsymbol{u})\rangle_{exp} - \langle f_\mu(\boldsymbol{u})\rangle_P \\ \Rightarrow \langle f_\mu(\boldsymbol{u})\rangle_{exp} &= \frac{1}{Z(\{\lambda_\nu\})} \sum_{\boldsymbol{u}} f_\mu(\boldsymbol{u}) \exp\left[-\sum_{\mu=0}^{K} \lambda_\mu f_\mu(\boldsymbol{u})\right], \end{aligned} \tag{1.25}$$

We now want to apply this approach to flocks. Flocks of birds are intrinsically out of equilibrium systems, and using the maximum entropy method to infer the probability distribution of flocks observables can appear risky, but recent results with networks of neurons [39, 42, 44], ensembles of amino acid sequences [32], and biochemical and genetic networks [30, 43], encouraged us to use the maximum entropy approach as a path for constructing statistical mechanics models of biological systems directly from real data. We saw in the previous sections that some relevant observables are the correlations of the orientations and speed fluctuations. Let's start considering as input observable for the maximum entropy method the flight directions (orientations), we shall add the speeds at a second stage.

Let's then identify $\boldsymbol{u}_i = \boldsymbol{v}_i/|\boldsymbol{v}_i|$ as in equation (1.7), and $f_\mu(\boldsymbol{u}) = C_{ij} = \boldsymbol{u}_i \cdot \boldsymbol{u}_j$. Then replacing λ_μ with $-J_{ij}$, we can rewrite equation (1.23) as

$$P(\boldsymbol{u}) = \frac{1}{Z(\{J_{ij})} \exp\left[\frac{1}{2}\sum_{i=1}^{N}\sum_{j=1}^{N} J_{ij}\boldsymbol{u}_i \cdot \boldsymbol{u}_j\right]. \tag{1.26}$$

Now $\{J_{ij}\}$ are the parameters to be adjusted to satisfy $\langle \boldsymbol{u}_i \cdot \boldsymbol{u}_j\rangle_P = \langle \boldsymbol{u}_i \cdot \boldsymbol{u}_j\rangle_{exp}$.

$P(\boldsymbol{u})$ has a a familiar form for physicists when written as:

$$P(\boldsymbol{u}) = \frac{1}{Z(\beta)} e^{-\beta E(\boldsymbol{u})}. \tag{1.27}$$

If a system has states described by the variable $\boldsymbol{u}$ and each state has energy $E(\boldsymbol{u})$, then equation (1.27) is the equilibrium distribution. The equilibrium distribution of equation (1.26) is a distribution whose energy is determined by the mutual alignment between birds, for $J > 0$ energy is lowered when the birds are aligned. This mechanistic interpretation is compatible with the common assumption that birds interact aligning to each other. Considering a system with Hamiltonian

$$\mathcal{H}(\{\boldsymbol{u}_i\}) = -\frac{1}{2}\sum_{i=1}^{N}\sum_{j=1}^{N} J_{ij}\boldsymbol{u}_i \cdot \boldsymbol{u}_j, \tag{1.28}$$

we would obtain

$$\frac{\mathrm{d}\boldsymbol{u}_i}{\mathrm{d}t} = -\nabla\mathcal{H}(\{\boldsymbol{u}_i\}) = \sum J_{ij}\boldsymbol{u}_j, \tag{1.29}$$

that is the basic interaction rule used in many models, starting from the Vicsek one.

Solving this problem for the full interaction matrix J is not very meaningful, particularly because birds are moving, the matrix J and the correlations C_{ij} are changing from an instant to the other, so that it is not possible to define a static distribution for C. However, if we consider the average correlation among pairs within a neighbourhood of size n_c

$$C_{int} = \frac{1}{N}\sum_{i}\frac{1}{n_c}\sum_{j\in_c}\left\langle \boldsymbol{u}_i \cdot \boldsymbol{u}_j \right\rangle, \tag{1.30}$$

then this quantity is stationary in time. Mathematically we have restricted the problem to two parameters J and n_c, indeed the maximum entropy distribution consistent with the observable C_{int} is given by:

$$P(\boldsymbol{u}) = \frac{1}{Z(J, n_c)} \exp\left[\frac{J}{2}\sum_{i=1}^{N}\sum_{j\in n_c^i} \boldsymbol{u}_i \cdot \boldsymbol{u}_j\right]. \tag{1.31}$$

Now, for a given value of n_c, J has to be adjusted so the expected value of C_{int} computed with the distribution (1.31) is equal to the experimentally measured one. This can be done using a low temperature expansion (spin wave approximation) to compute the partition function, and numerically solving the equations for n_c and J (for details see [9]).

In general there is a clear optimum value for n_c that can be therefore interpreted as the actual interaction range compatible with the measured correlations. Once the parameters are fixed, the model is fully determined. In [9] we showed that the model not only reproduces C_{int} as it should, but it also correctly predicts the full two-point and four-point correlation functions of the orientations on all scales. This indicates that alignment is indeed a crucial ingredient in flocking. More importantly we can study the dependence of the interaction range, the optimal n_c, from the density of the flock (Fig. 1.11) we find no correlation (constant n_c), providing a confirmation of the topological interaction with an analysis technique completely different from the one described in the previous paragraphs. We notice that the value of n_c obtained by the maximum entropy approach is larger than the one obtained with the anisotropy ($n_c \sim 21$) by a factor of order 3. In the next section I will address again this point.

Finally we must stress that the input observables are not the the full correlations, but C_{int}, that is restricted to the neighbouring birds. However the two point and four point correlation functions can be reconstructed with high accuracy using the maximum entropy probability distribution. Therefore the theory gives the right predictions (this is shown in figure 1.13 for the correlation function of the speed fluctuations).

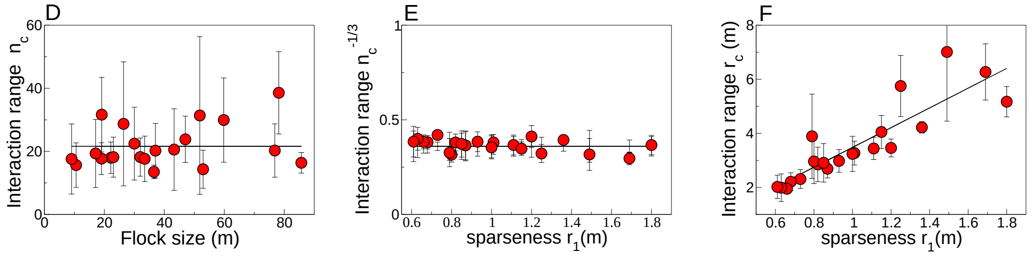

(a) (b) (c)

Fig. 1.11: (a) Inferred topological interaction range versus flock size, (b) Inferred topological interaction range versus sparseness and (c) inferred metric interaction range versus sparseness. Analogously to figure 1.3 the topological interaction range doesn't depend on the density, while the metric one does. This is an independent confirmation of the topological nature of the interaction. Figure from [9].

1.3.2 Numerical test of the maximum entropy approach

In the previous section I described how we applied the maximum entropy method to flock data. This method had always been applied to cases of static networks, while, as I discussed, flocks have a dynamical network. Therefore we wanted to check that all the methodology and the theory worked in the case of active out-of-equilibrium systems. We already showed that the theory gives the right predictions for the $c(r)$, now we focus on the significance of the inferred parameters J and n_c.

To do so, I considered the balanced topological model introduced in section 1.2.3. In this model the interaction of individuals is mainly based on alignment, it is suitable for obtaining reasonably realistic flocks that simultaneously grant cohesion and unstructured 3d distribution, and allows to vary the number of interacting neighbours of a bird.

These ingredients are enough to perform a test on the maximum entropy method. I simulated *realistic* flocks moving in three dimension with different interaction ranges n_c; I then applied the maximum entropy analysis to the synthetic data obtained and compared the inferred pairs (j^{mem}, n_c^{mem}) with the simulation ones (j^{sim}, n_c^{sim}).

The results of this comparison are shown in figure 1.12. I found for both J and n_c that the maximum entropy method returns overestimated values by a factor of 2.2 and 2.7 respectively. Nevertheless I found an excellent linear dependence between the real and inferred values of the parameters. Showing that the inference procedure works well, apart from a renormalization factor.

A possible argument to explain the overestimation of J and n_c reside in the dynamic feature of the interaction network, that possibly enhances the effectiveness of the interactions. When birds move move through the flock, they may encounter new neighbours before losing memory of the earlier flight directions and in so doing propagate information and correlation more effectively than if they were sitting on a fixed network. On the other hand in the maximum entropy model, interactions are static by construction, so the dynamical nature of the true interaction network is compensated by giving a larger effective value of n_c.

If we use the proportionality factor obtained from the real and inferred simulation parameters to rescale the parameters inferred for the birds we find the value $n_c \sim 8$ that is compatible with the one obtained from the study of anisotropy. We therefore had an independent confirmation not only for the

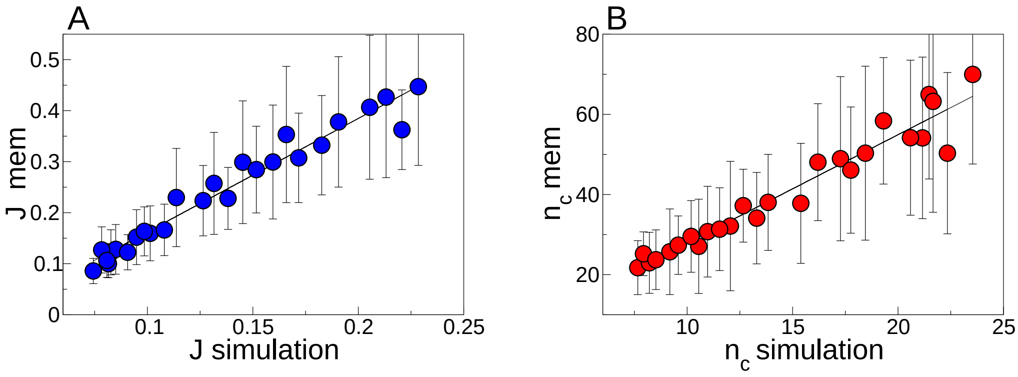

(a) **(b)**

Fig. 1.12: Comparison between the inferred parameter J (left) and n_c (right) and the corresponding simulation values. The excellent proportionality confirms the applicability of the maximum entropy method to an out-of-equilibrium system, while the proportionality factor of $\sim 1/3$ can be interpreted as an effect of the continuous modification of the interaction network. Figure from [9].

topological nature of the interactions, but also for its range.

1.3.3 Maximum entropy for the full velocities

Following the same method used for the orientation correlations, it is possible to infer the probability distribution for the full velocities [8], including also the speed degrees of freedom. In this case we must look for the maximum entropy distribution consistent with the following local correlation:

$$Q_{int} = \frac{1}{2v_0^2 N} \sum_{i=1}^{N} \frac{1}{n_c} \sum_{j \in n_c^i} |\boldsymbol{v}_i - \boldsymbol{v}_j|^2. \tag{1.32}$$

where we changed notation to stress that $\boldsymbol{v}_i$ are now the full velocities of the birds, (e.g. including direction and speed).

We also want the distribution consistent with the measured average speed of birds $V = (1/N)\sum_i v_i$, and its variance (fixing the mean squared speed $V_2 = (1/N)\sum_i v_i^2$). The maximum entropy consistent with Q_{int}, V and V_2 has the form,

$$P(\{\boldsymbol{v}_i\}) = \frac{1}{Z} \exp\left[-\frac{J}{4v_0^2} \sum_{i,j=1}^{N} n_{ij} |\boldsymbol{v}_i - \boldsymbol{v}_j|^2 + \frac{\mu}{v_0} \sum_{i=1}^{N} v_i - \frac{g}{2v_0^2} \sum_{i=1}^{N} v_i^2 \right], \tag{1.33}$$

with three parameters J, μ and g that have to be adjusted to fit the experimental data for a given connectivity n_c.

An interesting result concerns the inferred value of g, that is always near to zero. To explain why this is interesting we need to introduce the Hamiltonian derived from the mechanistic interpretation of $P(\{\boldsymbol{v}_i\})$

$$\mathcal{H}(\{\boldsymbol{v}_i\}) = \frac{J}{4v^2} \sum_{i,j=1}^{N} n_{ij} |\boldsymbol{v}_i - \boldsymbol{v}_j|^2 + \frac{g}{2V^2} \sum_{i=1}^{N} (v_i - V)^2, \tag{1.34}$$

The first term in this Hamiltonian describes the tendency of the individual velocities to adjust both direction and modulus to their neighbours, while the second term forces the speed to have, on average, the value V. From this perspective, we can interpret J as the stiffness of an effective “spring” that ties each bird’s velocity to that of its neighbours, and g as the stiffness of a competing spring that ties each speed to the desired mean i.e. to satisfy some physical constraint. Larger J means a tighter connection to the neighbours, and larger g means a tighter individual control over speed.

We have, in the limit of g going to infinity, that equation (1.34) reduces to (1.28), while it can be shown that $g = 0$ represents a critical point for the system, with the correlation length going as $\xi \sim r_1\sqrt{Jn_c/g}$, where r_1 is the average nearest neighbour distance (Fig. 1.13).

The low inferred value of g represents therefore a strong indication to the idea that the scale free correlations of speed fluctuations is the consequence of being near criticality.

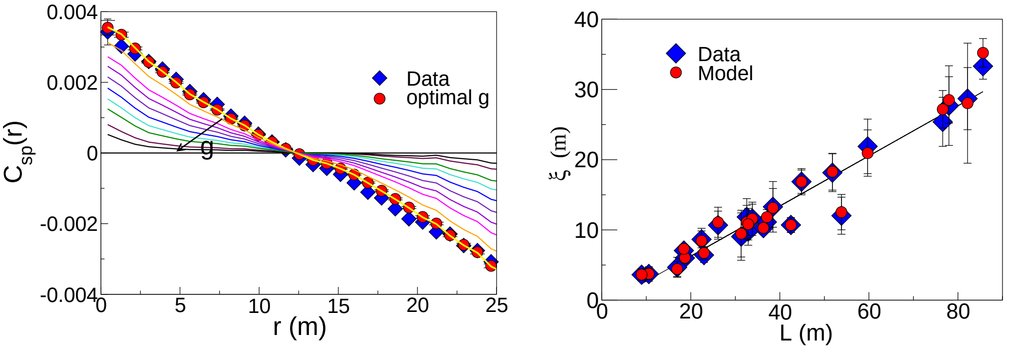

(a) **(b)**

Fig. 1.13: **(a)** Inferred correlation function of the speed fluctuations, for different values of the control parameter g (increasing in the direction of the arrow). **(b)** Correlation length, defined as the point where the correlation function crosses zero, in flocks of different sizes, for the experimental data (blue diamonds) and for the inferred model (red circles). Figure from [8].

1.3.4 A new flocking model with variable speed

The maximum entropy model gives us an instantaneous (static) probability distribution that is compatible with the observed data, and allows to infer the parameters describing the system with high accuracy. It predicts the right full correlation functions having as input just the short range correlation between neighbouring birds. Nevertheless it doesn't account for the dynamical evolution of the system, that implies a continuously changing interaction network.

To understand what happens when the full dynamical behaviour is taken in account we can bring inspiration from the mechanistic interpretation we talked about in previous paragraphs, and define of a novel model, whose equation of motion is the Langevin equation relative to the Hamiltonian (1.34).

$$\begin{aligned}\gamma\frac{\mathrm{d}\boldsymbol{v}_i(t)}{\mathrm{d}t} &= -\frac{J}{2v_0^2}\sum_j n_{ij}(\boldsymbol{v}_i-\boldsymbol{v}_j) - \frac{g}{v_0^2}\frac{\boldsymbol{v}_i}{v_i}(v_i-\hat{v}) \\ &\quad + \frac{1}{n_c}\sum_{j\in n_c^i}\boldsymbol{f}_{ij} + \boldsymbol{\eta}_i(t) \qquad (1.35)\\ \frac{\mathrm{d}\boldsymbol{x}_i(t)}{\mathrm{d}t} &= \boldsymbol{v}_i. \qquad (1.36)\end{aligned}$$

where we added the term $\boldsymbol{f}_{ij}$ to guarantee the cohesion of the flock, and the term of noise $\boldsymbol{\eta}_i(t)$, a normally distributed random vector delta correlated in time $\langle \eta_i^\alpha(t)\eta_j^\beta(t')\rangle = 2\gamma T\delta_{i,j}\delta_{\alpha,\beta}\delta_{t,t'}$, where $\alpha,\beta = x,y,z$, and T is an effective temperature.

Using only the equation (1.35) on a fixed lattice (and with no attraction–repulsion terms) we would obtain a spin–like model perfectly described by the probability distribution (1.33). Our goal is to investigate the dynamical behaviour obtained adding the equation (1.36).

Despite its similarity with other SPP models, the model I'm considering has a crucial new ingredient, namely that the speeds of the individual birds are not fixed but can change in time. Accordingly, equations (1.35) and (1.36) describe the evolution of the full velocity (rather than just the flight direction), with a term proportional to g that sets the scale of the speed fluctuations. In addition, existing SPP models are usually defined as discrete dynamical update equations, which do not have a well defined continuum limit. In contrast, I have defined the model as a stochastic differential equation.

I simulated the model using a finite interval (Euler) discretization [12], ob-

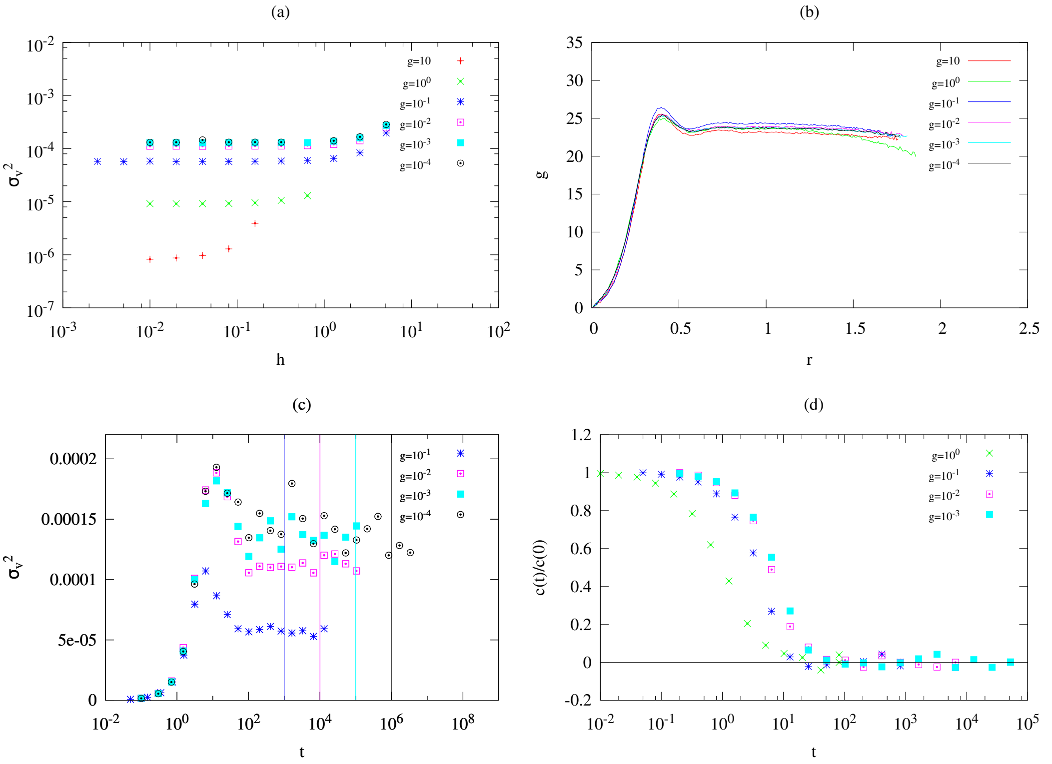

Fig. 1.14: Determining the simulation parameters. (a) The variance of the speed σ_v^2 should not depend by the integration time-step h. The optimal value of h is the highest in the region where $\sigma_v^2(h)$ is flat. **(b)** The parameter α in equation (1.39) determines the shape of the $g(r)$; the value $\alpha = 0.95$ grants a realistic structure as in comparison with figure 1.2. **(c)** The transient of $\sigma_v^2(g, t)$, the data sampling is started at $t_0 = 100/(hg)$ corresponding to the vertical lines in the plot. **(d)** Autocorrelation times; the sampling interval was chosen as $\Delta t = 10^3$ so that so that $c_v(t_{\Delta t}) = 0$ is satisfied for each value of g.

taining the following discrete equations.

$$\begin{aligned}\boldsymbol{v}_i(t+h) = \boldsymbol{v}_i(t) + h\frac{J}{2v_0^2}\sum_j n_{ij}(\boldsymbol{v}_j(t) - \boldsymbol{v}_i(t)) - h\frac{g}{v_0^2}\frac{\boldsymbol{v}_i}{v_i}(v_i - v_0) + \\ h\frac{1}{n_c}\sum_{j\in i}\boldsymbol{f}_{ij}(t) + \sqrt{h}\boldsymbol{\eta}_i(t) \end{aligned} \tag{1.37}$$

$$\boldsymbol{x}_i(t+h) = \boldsymbol{x}_i(t) + h\boldsymbol{v}_i(t).,\tag{1.38}$$

with,

$$\boldsymbol{f}_{ij} = \alpha\frac{\boldsymbol{r}_{ij}}{r_{ij}}\begin{cases}\frac{1}{4}\frac{r_{ij}-r_e}{r_a-r_c} & \text{if } r_{ij} < r_a \\ 1 & \text{otherwise}\end{cases},\tag{1.39}$$

The choice of the integration time-step h requires carefulness. A value too high of h would produce a wrong integration of the equations of motion, but reducing it means longer simulation times. A safe value of h can be obtained computing the variance σ_v^2 of the speed, that in principle should not depend by the integration time-step. In figure 1.14a the value of $\sigma_v^2(g,h)$ is plotted against h for different values of g. Decreasing h corresponds to a decrease of σ_v^2 until a steady value is reached. I choose the maximum value of h in the flat region of $\sigma_v^2(h,g)$; this value is also dependent by g, the higher is g, the lower is the corresponding maximum value of h. I found that a reasonable compromise, in the range of interest of g was $h = min(0.1, 0.005/g)$.

Even tough the model is intrinsically out of equilibrium, it reaches a stationary state for long enough times after the simulation start; we are interested to study the model in this stationary regime. In figure 1.14c I show the time dependence of $\sigma_v^2(g,t)$ from time, when the initial condition of $v_i = v_0\ \forall i$. $\sigma_v^2(g,t)$ grows from zero to a first peak until it relaxes to a stationary value. I choose the transient time after the initial conditions as $t_0 = 100/(hg)$, and started to record the simulation data after this transient.

To study the correlation function it's important to average over uncorrelated samples of the system. This can be done running as many different simulations as the number of samples needed to obtain a good statistics, or, more reasonably, to compute the (time dependent) autocorrelation

$$c_v(t) = \frac{1}{N}\frac{\sum_{i=1}^N v_i(0)v_i(t)}{\sigma(v(0))\sigma(v(t))},\tag{1.40}$$

of the birds and determine the sampling interval $t_{\Delta t}$ so that $c_v(t_{\Delta t}) = 0$ (Fig. 1.14d).

Finally, recalling that the term of attraction repulsion force $\boldsymbol{f}_{ij}$ was added to grant cohesive flocks and is absent from the maximum entropy theory, I adjusted the simulation parameter α of equation (1.39) in order to reproduce in figure 1.14b the experimental spatial distribution $g(r)$ of figure 1.2, so that the effect of this extra term was the most realistic possible.

With all other parameters fixed, I varied g, with the results shown in figure 1.15.

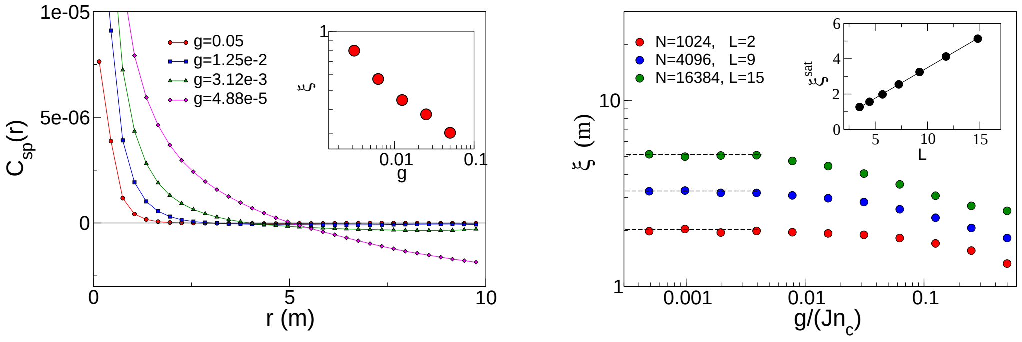

(a) **(b)**

Fig. 1.15: Simulations of the dynamical model. **(a)** Correlation function of the speed fluctuations at different values of g, in a flock of $N = 16384$ birds. Inset: Correlation length, measured from the exponential decay of the correlation functions at small r, as a function of $g/(Jn_c)$. **(b)** For smaller g, correlation lengths are measured from the zero crossing of the correlation function. For $g/(Jn_c) \ll 1$, ξ approaches a maximum value that depends on the size of the system. Inset: low-g maximum of ξ, as a function of the system size; the linear dependence of ξ on L is typical of scale–free behaviour. Figure from [8].

As expected from the analysis of the (static) maximum entropy model, the fluctuations in speed have a correlation length that grows as g is reduced. If g is not too small, we see correlations that decay exponentially, and the correlation length varies with $g/(Jn_c)$ as expected. When g is lowered even further, the exponential decay is modified by finite size corrections, and the correlation length, computed as the zero–crossing point of the correlation function, keeps increasing until a maximal, size dependent saturation value is reached. In this regime, the correlations extend over a distance determined by the system size, and ξ in fact grows linearly with L corresponding to scale–free behaviour (Fig 1.15b, inset).

This scenario confirms that the mechanism identified in the previous section produces scale–free correlations in the speed even when the full dynamical behaviour of the flock is taken into account.

2 Collective turns and information propagation in flocks

The maximum entropy approach indicates that flocks straight flight can be described by means of simple interaction rules based on alignment. The Vicsek model, which includes such rules, is an excellent base upon which it's possible to build models that reproduce many experimental evidences of real flocks. In fact real flocks change their flying direction, and they do it almost instantaneously at the naked eye observation. As I will discuss this is not a feature that the simple Vicsek model can reproduce. A recent analysis of the trajectories of turning flocks [3] shows that these changes of direction are not instantaneous; it propagates through the flock from a first turning bird to the last one. By studying collective turns we can therefore investigate one of the most important issues in collective behaviour, namely how information propagates through the system.

In this chapter I will first describe the experimental results on collective turns, then I will briefly explain how these results gave rise to a novel theory of flocking, and finally I will discuss the new model of flocking that I studied numerically, which is based on these recent findings.

2.1 Experimental results

To study turns, i.e. collective changes of directions, the full trajectories of all birds during the entire turning event are necessary (Fig. 2.1). From a rough analysis of these trajectories it's immediately evident that turns often occur in a plane, that is more or less parallel to the ground, and that trajectories curvatures have the same radius. Are they really simultaneous?

To answer the this question, we can study the modulus of the radial acceleration $a_i(t)$ of each bird (Fig. 2.1d); it has a clear peak whose position in time changes from bird to bird. We can therefore calculate the mutual turning

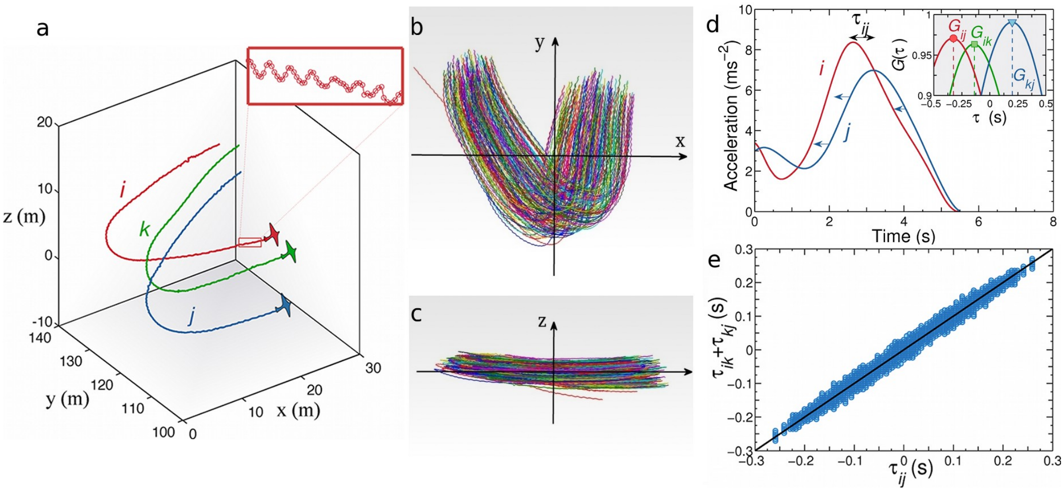

Fig. 2.1: Birds trajectories and turning delays. a, Reconstructed $3d$ trajectories of three birds belonging to a flock performing a collective turn. Sampling at 170Hz we capture fine details of the birds movement, such as the zig-zag due to wing flapping (10Hz in starlings - inset). **b, c,** Trajectories of all $N = 176$ birds of the same flock as in panel **a**. Each trajectory lies approximately on a plane, justifying a simplified planar description of the velocity. **d,** The radial acceleration of a turning bird displays a maximum as a function of time. In principle, given two birds i and j, one could simply define the turning delay τ_{ij} as the time shift between the peaks of their accelerations. In practice, due to experimental noise, using just one time point (the peak) gives an unstable estimate. To calculate τ_{ij} in a robust way the entire trajectories are necessary. This can be done by asking what is the delay τ_{ij} by which we have to time-shift the radial accelerations $a_j(t)$ to maximally overlap it with $a_i(t)$. This optimal shift corresponds to the time where the correlation function $G_{ij}(\tau) = \int dt\, \mathbf{a}_i(t) \cdot \mathbf{a}_j(t-\tau)$ reaches its maximum (inset). **e,** In the absence of experimental noise, for each triplet of birds, i, j, k we must have, $\tau_{ik} + \tau_{kj} = \tau_{ij}$: if i turns 20ms before k, and k turns 15ms before j, then i turns 35ms before j (Time Ordering Relation - TOR). Due to noise TOR will not hold strictly, but we still want it to be correct on average for τ_{ij} to make biological sense. We consider all triplets of birds and plot $\tau_{ik} + \tau_{kj}$ vs. τ_{ij}. The data fall on the identity line with relatively small spread, confirming the temporal consistency of the turning delays. Figure from [3].

delay τ_{ij} for each pair of birds; τ_{ij} will be greater than zero if bird i turned before j and vice versa. To do this with sufficient precision we need the full trajectories, in order to evaluate the cross correlation function between $a_i(t)$ and $a_j(t)$:

$$[a_i(t) \times a_j(t)](\tau) = \sum_{t=-\infty}^{\infty} a_i(t) a_j(t+\tau), \tag{2.1}$$

the delay τ_{ij} corresponds to τ of the maximum of equation (2.1), in othe words τ_{ij} is the time shift needed to obtain the maximum overlap between the acceleration curves.

Birds can now be ordered using these delays from the first who turned to the last one. This has to be done carefully, because the delays are not always consistent due to noise, e.g. given a triplet of birds i, j and k the time ordering relation (TOR) $\tau_{ij} + \tau_{jk} = \tau_{ik}$ is not always satisfied as it would have been in absence of noise. To overcome this frustration each bird is ranked according to the total number of times it *wins* (has a positive delay) against the other birds. The rank r_i of bird i is given by,

$$r_i = N - \sum_{j \neq i} 2 \left(\theta(\tau_{ij}) - \frac{1}{2} \right), \tag{2.2}$$

being $\theta(x)$ the step function.

The absolute turning time is then defined as

$$t_i = \frac{1}{r_i - 1} \sum_{r_j < r_i} (t_i + \tau_{ij}), \qquad r_i > 1. \tag{2.3}$$

From the rank versus absolute time plot (Fig. (Fig. **??**)a) we obtain a convex curve for early time, meaning that few birds started the turn, this few birds are also physically close to each other, so the start of the turn is localized in space, and the turning information is propagated through inter individual interaction.

To understand how the signal propagates through the flock, we need a dispersion law. If we assume that equally ranked birds have the same distance from the first turning bird, then we can define the distance travelled by the signal as the radius $x(t)$ of the sphere containing the first $r(t)$ birds in the rank, $x(t) = (r(t)/\rho)^{1/3}$ where ρ is the density of the flock. Since the birds are

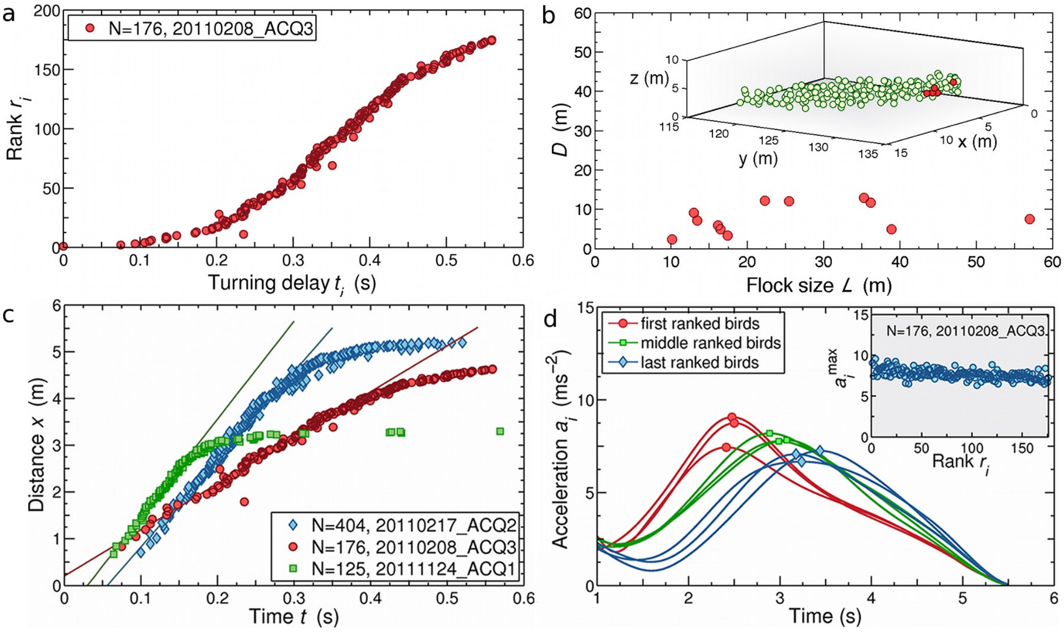

Fig. 2.2: **(a)** The rank r of each bird in the flock, i.e. its order in the turning sequence, is plotted vs its absolute turning delay t, i.e. the delay with respect to the top bird in the rank (the first to turn). The convex toe of the curve for early times indicates that few birds take initially the decision to turn. **(b)** The average mutual distance D between the top 5 birds in the rank does not increase with the linear size of the flock, L, hence indicating that the first birds to turn are actually close to each other in space. The result does not change using a different number of top birds. Inset: the actual position of the top 5 birds (red) within a real flock. **(c)** The distance x travelled by the information in a time t is proportional to the radius of the sphere containing the first $r(t)$ birds in the rank, namely $x(t) = [r(t)/\rho]^{1/3}$. The linear regime of $x(t)$ allows us to define a 'sound' speed of propagation, c_s, as the slope of $x(t)$ for early-intermediate times. The speed c_s varies significantly from flock to flock. **(d)** The intensity of the peak of the radial acceleration, $a^{\max}$, (solid symbols) decreases very weakly in passing from the first to the last turning birds. In the inset, we plot $a_i^{\max}$ vs the rank r_i for each bird. This slow decay indicates that the information propagates through the flock with negligible attenuation. Figure from [3].

moving off–lattice, this measure of distance is more robust with respect to a metric one, that would have to be taken in an arbitrary instant of time. The $x(t)$ curve has a clear linear regime before it saturates due to border effects; the distance travelled by information grows linearly in time, like a sound wave would do (Fig. 2.2c).

2.2 Theoretical modelling of information propagation in turns

What do existing models tell us about the experimentally measured linear propagation of information?

As we have seen in the previous chapter, the study of Vicsek-like models successfully explains many features of flocking, with even the model derived from the maximum entropy model belonging to the same category.

On large time and length scales these models are described by Toner and Tu hydrodynamical theory [45], and in a recent work [14] is presented a continuous theory coupling the Toner and Tu theory with the new inertial model that I will describe in this chapter. In the long wavelength limit (infinite system size and zero wave-number) the two theories are showed to be equivalent, the theory is universal and independent of the details of the microscopic dynamics. In this regime the propagating orientational modes are always coupled with density fluctuation.

But the flock turns we are studying are not in this regime. The turning events occur in very short time scales, with negligible mutual diffusion between the birds; The size of the flocks is relatively small ($N < 1000$) and, more important, we measured no propagation of density fluctuation. The theory described by Cavagna et al. in [14] reveals the emergence of a gap in the dispersion relation, and shows that propagation phenomena in flocks have a different nature in different size regimes: for large scales the propagation of orientations is coupled with density fluctuation as in the standard Toner and Tu theory, while for smaller scales a different kind of directional propagation is predicted, with a linear dispersion law, compatible with the one observed in real flocks; it is also predicted that at an intermediate range of system sizes no propagation can occur at all.

In general any coarse grained theory is independent on the microscopic details only in the thermodynamic limit. For finite sizes and time scales the microscopic details of the dynamics are in fact crucial. For this reason it is convenient to focus on a microscopic description of the system, like the one given by self-propelled particle models. The first thing one can realize is that, on short scales, the Vicsek model is not expected to exhibit propagation modes. To see this, we consider (in analogy to what we saw in section 1.3) a general continuous limit Hamiltonian for a Vicsek–like model,

$$\mathcal{H} = -J \sum_{<i,j>} \boldsymbol{v}_i \cdot \boldsymbol{v}_j, \tag{2.4}$$

that describes a system of interacting agents updating their velocity according to the social force $\boldsymbol{F}_i = \partial \mathcal{H} / \partial \boldsymbol{v}_i$.

To simplify the algebra we exploit the fact that the trajectories of birds during a turn lie approximately on a plane (Fig. 2.1b and c). This allows us to use a two-dimensional velocity, $\mathbf{v}_i = (v_i^x, v_i^y) = v\, e^{i\varphi_i}$, where the phase φ_i is the angle between the direction of motion of i and that of the flock (we make the standard assumption that v is constant). In the highly ordered phase the velocities $\mathbf{v}_i$ differ little from the collective one, so that $\varphi_i \ll 1$. We can thus expand $\mathcal{H}$ in equation (2.4). [9],

$$\mathcal{H} = \frac{J}{2} \sum_{\langle ij \rangle} (\varphi_i - \varphi_j)^2 = \frac{1}{2} a^2 J \int \frac{d^3x}{a^3} \left[\boldsymbol{\nabla} \varphi(x,t) \right]^2 \ , \tag{2.5}$$

where a is the average nearest neighbours distance and a term v^2 has been reabsorbed into J. The Langevin equation associated to Hamiltonian (2.5) is,

$$\frac{\partial \varphi}{\partial t} = -\frac{\delta H}{\delta \varphi} = a^2 J\, \nabla^2 \varphi \ . \tag{2.6}$$

Relation (2.6) is a diffusion equation for the phase φ, and it has dispersion law $\omega = ik^2$. This result has two consequences, both in sharp contrast with the empirical data: **i)** information travels much slower than linearly, $x \sim \sqrt{t}$, at variance with the linear propagation we find in turning flocks; **ii)** the frequency is imaginary, meaning that this is a non-propagating mode. Transfer of information gets damped exponentially in space and time, again in stark disagreement with the brisk, undamped propagation we observe in flocks.

This general argument is telling us that some critical ingredient is missing from Vicsek–like models. It is necessary to develop a novel theory.

2.2.1 The Inertial Spin Model: a new model for self-organized motion

The standard theory has two problems. First, it seems to be missing some conservation law. Hamiltonian (2.4) is invariant under rotation of the velocities $\mathbf{v}_i$ ($\varphi_i \to \varphi_i + \delta\varphi$); all directions of flight are equivalent for a flock. Through Noether's theorem, a symmetry implies in general a conservation law, of which, however, there is no trace in the standard theory. As a consequence a quantity that should be conserved is instead relaxed and not transported across the flock. Second, equation (2.6) completely neglects behavioural inertia, as the social force, $F_\mathrm{s} = aJ\nabla^2\varphi$, controls directly $\dot{\varphi}$, rather than $\ddot{\varphi}$. This is odd: imagine that the interaction with the neighbours requires bird i to perform a U-turn in one time step. This behaviour is allowed by the standard theory, although it is clearly unreasonable.

In Attanasi et al. [3], a novel flocking theory is presented, showing that considering the proper conservation law, and introducing a *behavioural inertia* it is possible to explain the observed propagation of information and predict a non trivial relation between polarization and speed of propagation.

Here I will follow the approach of [17] where a novel dynamical model reproducing the experimental information transfer is discussed.

Even if the system as a whole (considering velocities and positions of the birds) is not Hamiltonian, if we focus solely on the velocities, we can try to describe it with a constrained deterministic model. Let's start imposing a constrain that fixes the modulus of the velocity $|\boldsymbol{v}_i| = v_0$, and defining the Hamiltonian of a system of interacting (by alignment) particles, that embodies the conservation law for the generator of the velocity rotation. Let me stress that we are considering rotations in the *internal* space of velocities and not, as usual, in the external space of positions (i.e. the rotation of the velocity vector and not of the position one). If we call $\boldsymbol{s}_i$ the local generator of rotations of the velocity $\boldsymbol{v}_i$ of bird i (i.e. internal momentum conjugated to the phase ϕ_i), then the Hamiltonian reads as,

$$\mathcal{H}(\boldsymbol{v}, \boldsymbol{s}) = -\frac{J}{2v_0^2}\sum_{ij} n_{ij}\boldsymbol{v}_i \cdot \boldsymbol{v}_j + \frac{1}{2\chi}\sum_i \boldsymbol{s}_i^2 \ , \tag{2.7}$$

where the first term is the familiar alignment interaction, while in the second term we have a kinetic term with a generalized moment of inertia χ quantifying the resistance of a bird to a change of its spin. The global internal angular momentum $\sum_i \boldsymbol{s}_i$ is a conserved variable.

The (deterministic) equation of motion derived from 2.7 are,

$$\frac{d\boldsymbol{v}_i}{dt} = \boldsymbol{v}_i \times \frac{\partial \mathcal{H}}{\partial \boldsymbol{s}_i} = \boldsymbol{v}_i \times \frac{1}{\chi}\boldsymbol{s}_i \tag{2.8}$$

$$\frac{d\boldsymbol{s}_i}{dt} = -\boldsymbol{v}_i \times \frac{\partial \mathcal{H}}{\partial \boldsymbol{v}_i} = \boldsymbol{v}_i \times \boldsymbol{F}_i \tag{2.9}$$

$$\frac{d\boldsymbol{r}_i}{dt} = \boldsymbol{v}_i, \tag{2.10}$$

where we must note that $(\boldsymbol{v}_i, \boldsymbol{s_i})$ are not canonical variables; $\boldsymbol{s}_i$ is the conjugated moment to the phase $\boldsymbol{\varphi}_i$, not to the velocity vector $\boldsymbol{v}_i$. Equations (2.8) and (2.9) are obtained by the explicit relations between $\boldsymbol{v}$, $\boldsymbol{\phi}$ and $\boldsymbol{s}$ with the constrain of constant modulus velocity (see [17] for details).

When the spin is equal to zero, equations 2.8, 2.9 and 2.10 describe a system of particles moving in a straight line; while when $\boldsymbol{s}$ is different from zero, but constant, the vector $\boldsymbol{v}$ performs a uniform circular motion, resulting in a circular trajectory of constant radius $R \sim v_0\chi/|\boldsymbol{s}_i|$. Hence, the spin $\boldsymbol{s}_i$ has a clear kinematic meaning being related to the instantaneous curvature $\kappa = 1/R$ of the trajectory. When there are forces acting on the particle the local spin/curvature $\boldsymbol{s}_i$ changes in time, inducing a variation in the rate of direction changes. The paths followed by the particles in real space depend on the instantaneous realization of the forces.

However, the important point is that - whatever these forces are - in our new model they act on the spin $\boldsymbol{s}_i$ and not directly on the velocity $\boldsymbol{v}_i$. In other terms, forces cannot change the direction of motion abruptly, but there is an inertial effect mediated by $\boldsymbol{s}_i$. In this respect, we see that the generalized inertia χ measures the resistance of the particle to change the instantaneous radius of curvature of its trajectory.

Following the same argument of the last paragraph, we can easily check that this new model exhibits an undamped linear propagation of orientation information. For a strongly ordered flock we can write

$$\mathcal{H} = \frac{J}{4}\sum_{i,j} n_{ij}\left[\phi_i - \phi_j\right]^2 + \sum_i \frac{s_i^2}{2\chi} \sim J n_c a^2 [\nabla\phi]^2 + \sum_i \frac{s_i^2}{2\chi}, \tag{2.11}$$

where n_c is the average number of interacting neighbours $n_c = (1/N)\sum_{ij} n_{ij}$.

The deterministic equations reads in this case,

$$\begin{aligned}\frac{\partial\varphi}{\partial t} &= \frac{s}{\chi}\\ \frac{\partial s}{\partial t} &= n_c a^2 J \nabla^2 \varphi.\end{aligned} \tag{2.12}$$

and retrieve the d'Alambert's equation from the second derivative of ϕ,

$$\chi \frac{\partial^2 \varphi}{\partial t^2} = J n_c a^2 \nabla^2 \varphi \ . \tag{2.13}$$

This equation can be easily solved in Fourier space to get the dispersion relation, namely the law describing how directional information travels through the system. We find,

$$\omega = c_s k \ , \tag{2.14}$$

with $c_s = \sqrt{J n_c a^2/\chi}$. A real value for the frequency ω corresponds to propagating modes: what we find is therefore that a deterministic flock exhibits undamped propagating modes of the phase. Besides, the dispersion law is linear, meaning that propagating modes travel at a well defined speed c_s, which is a function of the alignment strength and the generalized inertia. Linear propagation is reminiscent of sound propagation in a medium. Here, however, the modes that we are looking at are not related to density fluctuations, but to phase fluctuations. In fact the same equations for the phase we are looking at, and the same dispersion law, would also hold for a fixed network of particles, e.g. a regular lattice. Phase propagating modes mean that if in a flock a particle starts turning, this change will affect through the alignment term the spin/curvature of nearby particles, which will start turning themselves, and the whole system will perform a collective turn.

The deterministic model we have just introduced conserves spin (through the continuity equation), but it does so a bit too effectively, as in absence of forces the angular velocity remains forever constant.

This is easily solved adding a dissipative term coupled with $\boldsymbol{s}$, and associating it to a noise term, making the model stochastic,

$$\frac{d\boldsymbol{v}_i}{dt} = \frac{1}{\chi}\boldsymbol{s}_i \times \boldsymbol{v}_i \tag{2.15}$$

$$\frac{d\boldsymbol{s}_i}{dt} = \boldsymbol{v}_i(t) \times \left[\frac{J}{v_0^2}\sum_j n_{ij}\boldsymbol{v}_j - \frac{\eta}{v_0^2}\frac{d\boldsymbol{v}_i}{dt} + \frac{\boldsymbol{\xi}_i}{v_0} \right] \tag{2.16}$$

$$\frac{d\boldsymbol{r}_i}{dt} = \boldsymbol{v}_i(t), \tag{2.17}$$

with $\boldsymbol{v}_i \cdot \boldsymbol{s}_i = 0$. Here η is a generalized viscous coefficient and $\boldsymbol{\xi}_i$ is an normally distributed vectorial noise with variance

$$\langle \boldsymbol{\xi}_i(t) \cdot \boldsymbol{\xi}_j(t') \rangle = (2d)\,\eta\, T\, \delta_{ij}\delta(t-t')\ , \tag{2.18}$$

where we have introduced the generalized temperature T, in analogy to physical systems. Note that, the constraint $|\boldsymbol{v}_i| = v_0$ is satisfied by these equations.

Finally we must explain the role of dissipation. We already saw that in the deterministic limit $\eta \to 0$ we get linear propagation of all possible modes $\omega = c_s k$. At the opposite limit $\chi/\eta^2 \to 0$ we retrieve the Vicsek model limit, with purely imaginary ω and diffusive dispersion law.

In the general case, where both dissipation and inertia are different from zero, we obtain

$$\omega = i/\tau \pm \omega_0\sqrt{1 - k_0^2/k^2}\ , \tag{2.19}$$

with

$$k_0 \equiv \frac{\eta}{2\sqrt{J n_c a^2 \chi}} \quad , \quad \tau \equiv 2\chi/\eta\ , \tag{2.20}$$

and where $\omega_0 \equiv c_s k$ is the zero dissipation frequency. k_0 and τ are the two relevant scales, respectively in wave number and time, related to the effect of dissipation.

2.2.2 Numerical simulations

I implemented and studied the discrete version of equations (2.15), (2.16) and (2.17) with the twofold objective of checking the model's behaviour in the different regimes and compare the result with the experimental data.

The discrete equation of motion are,

$$\boldsymbol{v}_i(t+h) = \boldsymbol{v}_i(t) + \boldsymbol{v}_i(t) \times \frac{1}{\chi}\boldsymbol{s}_i(t)\, h \tag{2.21}$$

$$\begin{aligned}\boldsymbol{s}_i(t+h) = \boldsymbol{s}_i(t) + \boldsymbol{v}_i(t) \times \frac{J}{v_0^2}\sum_j n_{ij}\boldsymbol{v}_j(t)\, h \\ - \frac{\eta}{\chi}s_i(t)\, h + \boldsymbol{v}_i(t) \times \frac{\boldsymbol{\xi}_i(t)}{v_0}\sqrt{h}\end{aligned} \tag{2.22}$$

$$\boldsymbol{r}_i(t+h) = \boldsymbol{r}_i(t) + \boldsymbol{v}_i(t)\, h \tag{2.23}$$

where the in the equation for $\boldsymbol{v}$ the term $\mathrm{d}\boldsymbol{v}_i/\mathrm{d}t$ was replaced with $\boldsymbol{s}_i$. The noise variance is

$$\langle \boldsymbol{\xi}_i(t) \cdot \boldsymbol{\xi}_j(t') \rangle = (2d)\, \eta\, T\, \delta_{ij}\delta_{t,t'} \ . \tag{2.24}$$

The interaction range is given by the simple topological model described in the previous chapter: each particle interacts with its first n_c neighbours, the value of $n_c = 6$ was fixed in all the simulations.

To chose the proper value of h I proceed as in section 1.3.4. I computed the mean values and standard deviation of several quantities such as the deviation from the mean direction and the amplitude of the spin $|\boldsymbol{s}_i|$ for different values h. The clearest signal comes from the variance of the speed $\sigma^2_{|\boldsymbol{s}|}$, whose value typically decreases when h is decreased, until it reaches a steady, parameters dependent, value. I found that a reasonable value is $h = 0.1\sqrt{\xi/J}$, being $\sqrt{\xi/J}$ a characteristic time scale for the system (we have $c_s \propto \sqrt{J/\chi}$, or in analogy with an harmonic oscillator $\chi \equiv$ *mass* and $J \equiv$ *spring constant*, so that $\sqrt{J/\chi} \equiv resonant\ frequency$).

In real flocks turns start localized, namely from one bird (the initiator), and information propagates through the flock at a constant rate. However we don't know the reason why the initiator starts to turn; it may be because of some external perturbation, i.e. being threatened by a predator, or it can be the effect of random fluctuation. If we run simulations of the above model choosing the parameters so that the polarization is high ($\Phi > 0.95$) we eventually find global fluctuations of the mean direction of motion initiated by random fluctuation, but we will have no control on when this happens nor on the identity of the initiator; it is even unclear if we can call these fluctuation *turns*.

To study the role of the parameters η, χ and J in the propagation of directional information, I used an external perturbation directly acting on the direction of one (known) particle. The perturbation rotates the velocity vector $\boldsymbol{v}_0$ of bird "0" by a time dependent angle $\theta(t)$ whose aperture follows a smoothed ramp evolution rule,

$$\cos\theta(t) = \begin{cases} \frac{1}{2}\left[1-\cos\left(\pi(t-t_0)/T\right)\right] & \text{if } t_0 < t < T \\ 1 & \text{if } t > T \end{cases}, \tag{2.25}$$

where t_0 is the starting instant of the perturbation and T the duration of the ramp (see red line in Fig. 2.3d,e,f).

In the simulation the initial condition consisted in *flocks* of particles uniformly distributed in a sphere and perfectly aligned. The initial values of $\boldsymbol{s}$ is set to zero, so that the flock initially moves on a straight line. The system was simulated in open space (no boundaries). The radius of the initial sphere (and so the mean distance of interacting particles a) was chose so that the mutual diffusion of the particles was (roughly) realistic in the time scales of interest.

The perturbed particle is put in the centre of the flock, and the perturbation is applied after a short transient, necessary for the mean amplitude of $\boldsymbol{s}$ to reach a steady value. This choice of the transient does not assure that the system really reached a steady state, but I chose not to use an attraction repulsion term to avoid complications in the interpretation of the result, and in absence of an attraction repulsion term or boundaries we expect that the flock will evaporate in the infinite time limit, so I decided a value of the transient that assured a reasonable control on the volume of the flock. This compromise is not worrying since my objective was to study a phenomenon, the turn driven by a perturbation, that is intrinsically far from the steady state.

Finally the duration T of the ramp was chosen so that the delay between the initiator and the rest of the flock, calculated as in equation (2.3), was comparable with the delays observed in real flocks.

According to the analytical arguments given in the previous section, we expect two different regimes, defined by the values of η and χ:

1) **Overdamped regime:** $\eta^2/\chi > n_c J(a/L)^2$. In this regime, given a system of size L, some attenuated propagation occurs up to certain spatial scales ($k \geq k_0$, with $k_0 = 1/(2a\sqrt{n_c J \chi}) > 1/L$). On larger scales ($k < k_0$) however, dissipation takes over leading to an exponential decay of the signal. The extreme case occurs for $\eta^2/\chi \to \infty$ (or $\chi/\eta^2 \to 0$), corresponding to the Vicsek model, when propagation of orientational perturbations does not occur on any scale.

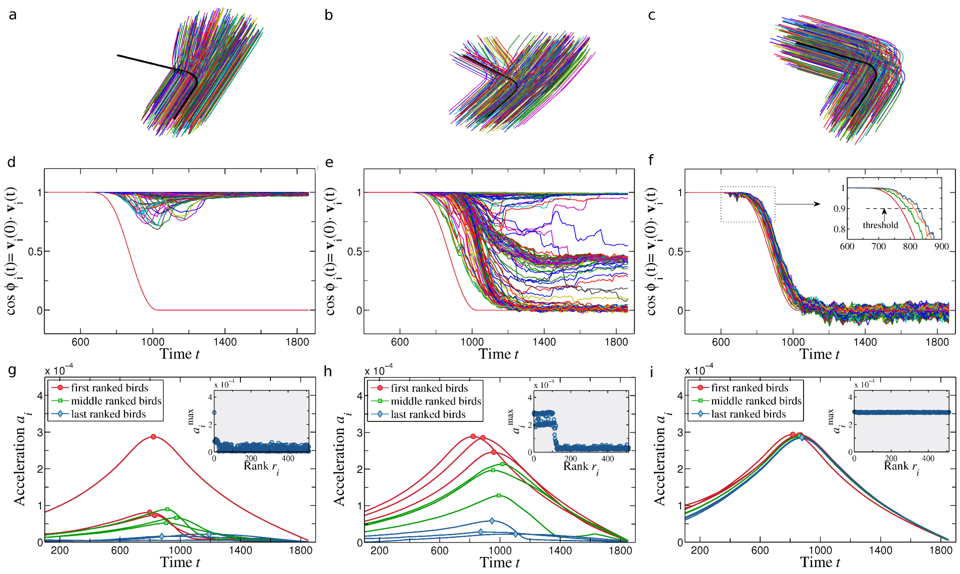

Fig. 2.3: Information propagation in different regimes. **a.** Strongly overdamped regime, $\eta^2/\chi = 28.8 \times 10^2$. The signal is quickly dissipated and there is no collective turn. The trajectory of the initiator is displayed as a thick black line. $\eta = 60$, $\chi = 1.25$, $J = 0.8$. **b.** Overdamped regime, $\eta^2/\chi = 1.8 \times 10^2$. Some propagation occurs, but the signal is strongly attenuated before reaching throughout the whole group. As a consequence, the flock looses cohesion and coherence while turning. $\eta = 15$, $\chi = 1.25$, $J = 0.8$. **c.** Underdamped regime, $\eta^2/\chi = 7.2 \times 10^{-2}$. The signal is propagated unattenuated through the whole flock, which performs a neat turn retaining shape and cohesion. $\eta = 0.3$, $\chi = 1.25$, $J = 0.8$. **d**, **e**, **f** Cosine of the individual velocities with the original flight direction of the flock for the three cases displayed in panels **a**, **b**, **c**. The cosine curve of the initiator is displayed as a red curve: at time $t = t_0$ the flight direction of the initiator is turned by 90 degrees following a smoothed ramp curve. The inset in panel **f** shows the threshold used to compute the ranking of the particles (see text). **g**, **h**, **i** Individual acceleration profiles for the three cases displayed in panels **a**, **b**, **c**. The acceleration curves have been low-pass filtered to cure noise and high frequency oscillations. The insets display the intensity of the peak as a function of rank. The other parameters of the simulations are $N = 512$, $T = 8 \times 10^{-5}$, $n_c = 6$, $v_0 = 0.1$. The integration time is chosen as $dt = 0.1\sqrt{\chi/J}$ to ensure proper simulation time for all values of J and χ. Figure from [17].

2) **Underdamped regime:** $\eta^2/\chi \ll n_c J (a/L)^2$. In this regime there is linear propagation of the signal throughout the whole system with negligible attenuation. The speed of information propagation is determined solely by the ratio between alignment strength and inertia, $c_s = a\sqrt{n_c J/\chi}$.

As a first step I qualitatively checked the emergence of the two expected regimes. To do so I fixed the values of temperature T, interaction strength J, moment of inertia χ and velocity modulus v_0, so that the system was strongly polarized, and the expected value of propagating speed c_s was fixed. Then I chose three values of the viscous coefficient in order to obtain underdamped, slightly overdamped, and strongly overdamped (Vicsek limit) regimes.

The simulation result are shown in figure 2.3, where it is immediately evident that in the two overdamped cases the perturbed particle was not followed by all the rest of the flock.

In the strongly overdamped regime (Fig. 2.3a), there are few particles affected by the perturbed one change of direction, but this effect is quickly dissipated as is evident from figure 2.3d where the cosine of the angle between the initial direction and direction at time t is plotted for all particles.

In the intermediate case (Fig. 2.3b), some of the neighbours of the initiator follow it, but information doesn't propagate to the entire flock, with the effect of damping still evident in the acceleration curves (panel h).

Finally in the underdamped case (Fig. 2.3c), the whole flock quickly changes its direction with very low damping effects.

This first positive result encouraged to carry on a deeper comparison with real flocks.

2.2.3 Comparison with experimental data

To compare the model and experimental data, I studied it in the underdamped regime, in condition of high polarization. In this regime, I quantify the dispersion law using the method introduced in section 2.1. I ranked all the particles according to their order of turning: the initiator has rank $r = 0$, then the particle that first starts turning after the initiator has rank $r = 1$ and so on. To determine the rank of a particle I followed two different procedures. I looked at the cosine curve (namely the dot product $\boldsymbol{v}_i(0)\cdot\boldsymbol{v}_i(t)$ shown in figure 2.3f) of the particle and determine its absolute turning delay from the initiator (and therefore its rank) as the time when the cosine reaches a threshold

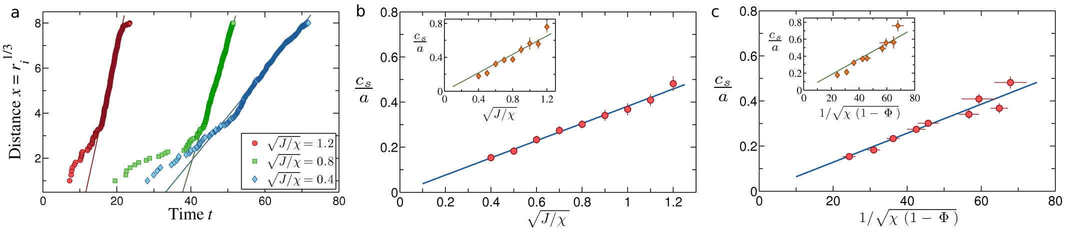

Fig. 2.4: Propagation curve and dispersion law. **(a)** Propagation curve. Distance x travelled by the turning front vs time, for three different values of the parameters η, χ, J in the small dissipation regime. The distance x travelled in a time t is proportional to the radius of the sphere containing the first $r(t)$ birds in the rank, namely $x(t) = [r(t)/\rho]^{1/3}$. $t = 0$ corresponds to the time when the initiator starts the turn. The three curves correspond respectively to $\eta = 0.3$, $\chi = 0.83$, $J = 1.2$ (red circles); $\eta = 0.3$, $\chi = 1.25$, $J = 0.8$ (green squares); $\eta = 0.3$, $\chi = 2.50$, $J = 0.4$ (blue diamonds). The rank is computed using the cosine curves (see text). The speed of propagation, c_s, is the slope of the propagation curve in linear regime. The coloured straight lines show the linear fits for the three different curves. **(b)** Speed of propagation c_s, normalized by the typical distance a of the interacting neighbours, as a function of $\sqrt{J/\chi}$. For each value of J/χ we run several simulations and estimate c_s from the slope of the propagation curve, the point corresponds to the average value and bars to standard error. The speed of propagation depends on the ratio J/χ as predicted by the analytic arguments in the previous section: more ordered flocks transmit the turning information quicker. Inset: same curve as in main panel, but using accelerations curves to compute ranks and propagation curves. **(c)** Speed of propagation c_s, normalized by a, as a function of $1/\sqrt{\chi(1-\Phi)}$. Inset: same curve as in main panel, but using accelerations curves to compute ranks and propagation curves. Figure from [17].

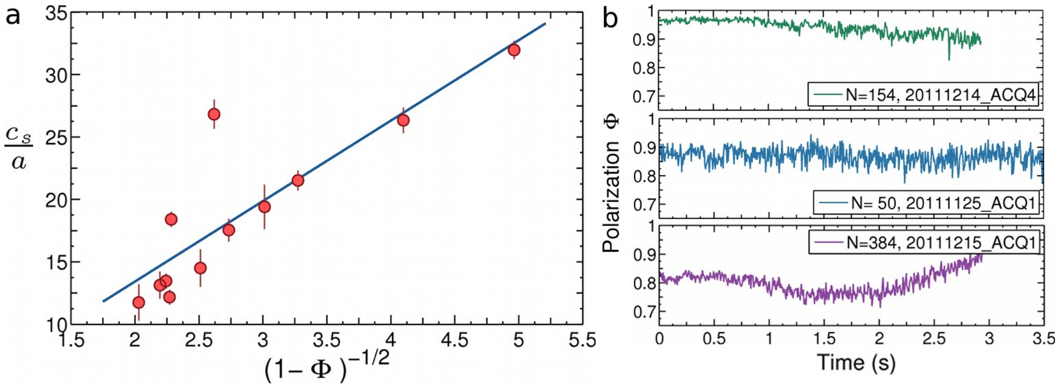

Fig. 2.5: Theoretical prediction in real flocks. a, The theory predicts that the rescaled speed of propagation of the turn, c_s/a, must be a linear function of $1/\sqrt{1-\Phi}$, where Φ is the polarization. The prediction is verified by the empirical data (P-value: $P = 3.1 \times 10^{-4}$; correlation coefficient: $R^2 = 0.74$). Each point is a different turning flock. **b**, Polarization as a function of time in three different flocks. The value of Φ reported in panel **a** corresponds to the time average over the entire duration of the turn. Figure from [3].

value (I choose 0.9 - see inset in figure 2.3f). Alternatively, I proceeded as in section 2.1: from the acceleration curves I computed the relative time delays between pairs of particles as the shift necessary to superimpose their curves (calculating the cross correlation function). Once the relative delays are found for all particles I ranked them accordingly to their mutual delays. The last method is more robust when it is not known a priori who is the initiator (as in experiments with real birds). The two procedures give equivalent results.

Looking at the rank as a function of delay time we get the ranking curve, describing how the turn is executed through the group; since the turn starts locally and the flock moves in three dimensions, $x(t) = r^{1/3}(t)$ is a measure of the distance x travelled by the turning wave in time t. As can be seen from figure 2.4a, $x(t)$ displays a clear linear dependence corresponding to a linear dispersion law, as predicted by the analytic argument in previous section.

The relation between the propagation speed and the parameters J and χ,

$$c_s = a\sqrt{\frac{n_c J}{\chi}}, \tag{2.26}$$

discussed in section 2.2.1 can be numerically verified. To do so, I ran numerical simulations for several values of the parameters in the underdamped regime. I fixed $\eta = 0.3$ and varied J and χ to obtain propagation curves with different slopes, but kept $J\chi$ constant in order to have the same value of $k_0 < 1/L$. I recall here that the condition for the underdamped regime is $\eta^2/\chi \ll n_c J(a/L)^2$, so in order to run simulation with different expected values of c_s, but in the same regime I changed the ration between J and χ keeping fixed their product, namely k_0. Then, for each simulation, I computed the $x(x)$ and estimated c_s as the slope obtained from a fit of the linear part of the curve (Fig. 2.4a). As can be seen from figure 2.4b, the dependence of c_s on J/χ is very well reproduced by numerical data.

Finally, the theory of Attanasi et al. [3] predicts a nontrivial relation between the propagation speed c_s and the polarization Φ: when the spin-wave approximation limit holds (as it is for birds) we have,

$$\frac{c_s}{a} \propto \frac{1}{\sqrt{(1-\Phi)\chi}}. \tag{2.27}$$

The relation between propagation speed c_s/a and $1/\sqrt{(1-\Phi)\chi}$ is shown in figure 2.4c. Also in this case the numerical data agree very well with the analytical prediction.

The behaviour displayed in figure 2.4 is analogous to what is observed in natural flocks of birds (Fig. 2.5). The propagation curves look indeed very similar to the ones computed for real flocks and shown in figure 2.2. Even more importantly, figure 2.4c is remarkably similar to what was found in real data, and the model correctly reproduces the experimentally found relationship between propagation speed and degree of order in the system. We can therefore conclude that Equations (2.15) , (2.16) ,(2.17) in the underdamped limit fully describe the correlated collective turning exhibited by real flocks. I remind that in this limit inertia and deterministic effects dominate over dissipation: it is the Hamiltonian structure of the dynamical equations, and the connected conservation law, that cause the linear dispersion law and the highly non-trivial relationship between speed of propagation and degree of order in the system.

3 Collective behaviour in Swarms of Midges

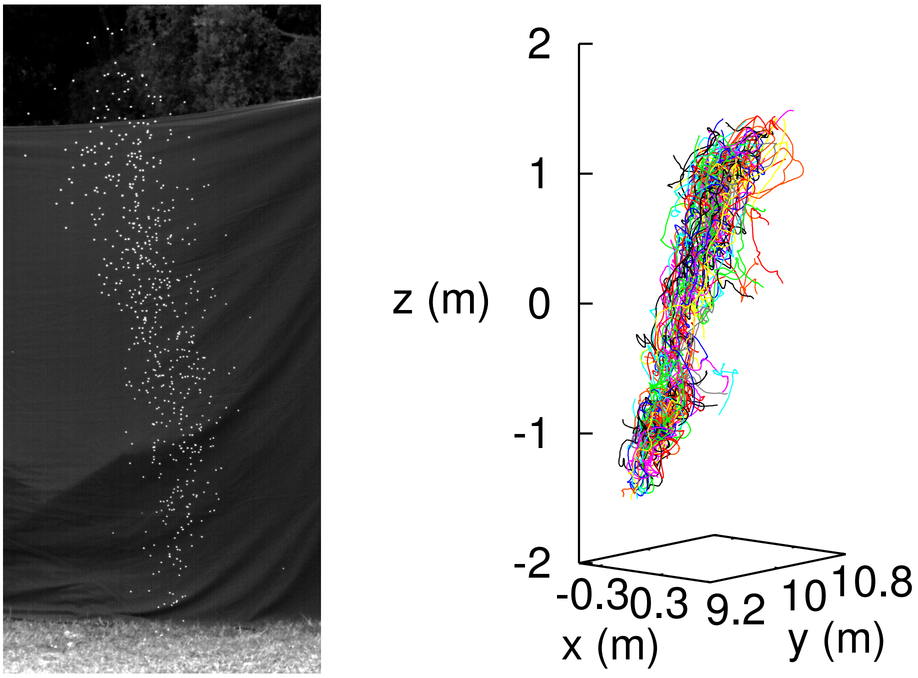

Fig. 3.1: Left A (cropped) frame from a midges acquisition. **Right** Reconstructed trajectories for the same acquisition.

In this chapter I describe a completely different biological system: insect swarms. While in birds the most striking evidence of collective behaviour is global alignment, a swarm of insects appears to be completely disordered. It is known [22] that the position where swarms of mosquitoes or midges form is strongly influenced by the surrounding environment. The probability of finding a swarm is significantly increased with the presence of a zone of high contrast between light and shade on the ground. The first question to be answered is whether the single insects interact with each other, or they are independently influenced only by the landmark.

A campaign of observations was performed in Rome in the 2012 and 2013 summer. Swarms of midges (Diptera:Chironomidae and Diptera:Ceratopogonidae) were filmed in several public parks where they find their natural habitat, and the individual trajectories were reconstructed with the same technique used for birds.

The study of correlation functions and susceptibility showed that the individual midges in the swarm do interact with each others, with a metric interaction range. The comparison with simulations of the Vicsek model enforced the idea that the swarms are spontaneously poised to the critical point of an order–disorder phase transition, leading to an estimate of the individual interaction range. In this chapter I will first describe the experimental results and then I will discuss the numerical analysis I performed on the critical behaviour of Vicsek model and how it helped us to understand what happens in natural swarms.

3.1 Experimental results

The first feature to be investigated in midges swarm is the degree of order. Swarms appear completely disordered to the naked eye, but they move very fast. Are they really disordered or there is something not captured by the human eye?

The standard order parameter normally used in collective behaviour is the polarization, $\Phi = (1/N)|\sum_i \boldsymbol{v}_i/v_i|$, where N is the number of midges in the swarm and $\boldsymbol{v}_i$ is the velocity of insect i. The polarization measures the degree of alignment of the directions of motion; it is a positive quantity and its maximum value is 1. The average polarization over all swarms is quite small, $\Phi \sim 0.21$ (Fig. 3.2). As a reference, in starling flocks we have $\Phi \sim 0.97$, on average (see section 1.1.3).

Clearly, swarms are not in a polarized state, but translation is not the only possible collective mode. For example, it is well-known that fish school can produce rotating (milling) configurations. Moreover, a group can expand/contract, giving rise to dilatational (or pulsive) collective modes. For this reason a

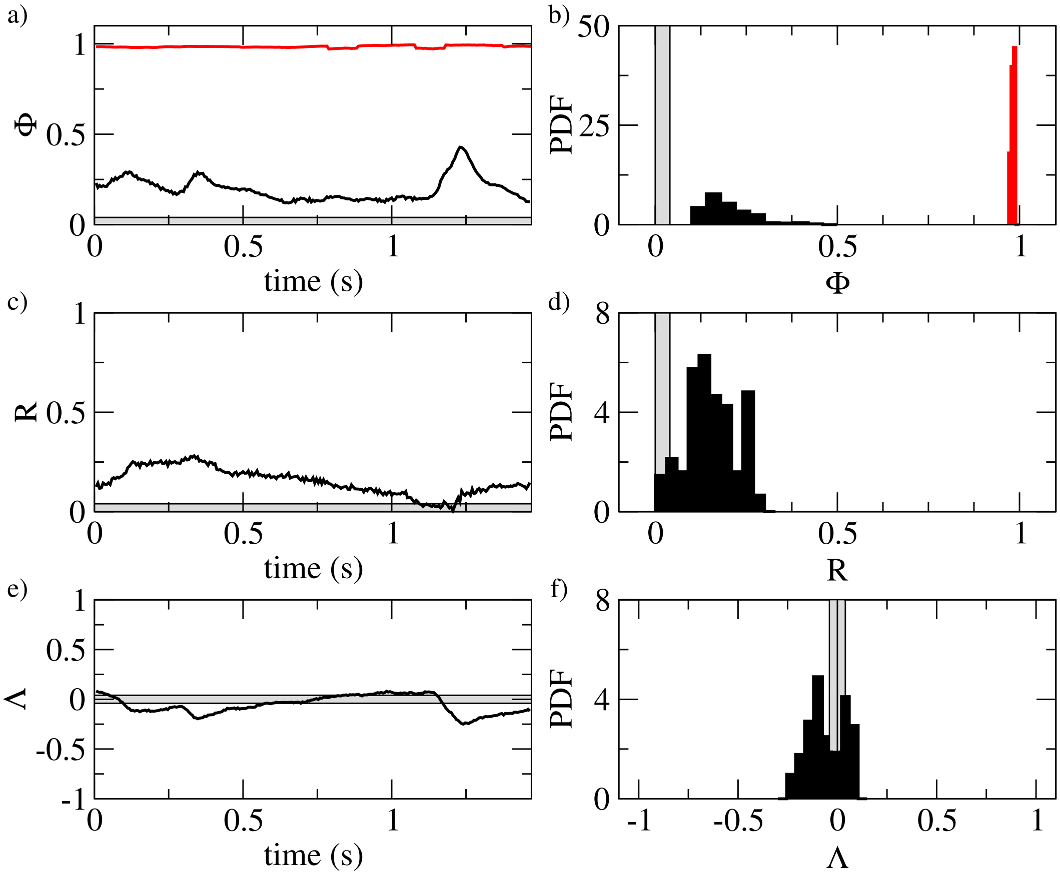

Fig. 3.2: Natural swarms lack global order. Order parameters in a typical natural swarm. In all panels the grey band around zero is the expected amplitude of the fluctuations in a completely uncorrelated system. The left panels are relative to the time series of the order parameters, the right ones to their probability distribution. **Top:** The alignment order parameter, known as polarization, $\Phi \in [0:1]$. In red is reported the reference value of the polarization in a flock of starlings. **Middle:** Rotational order parameter, $R \in [0:1]$. **Bottom:** Dilatational order parameter $\Lambda \in [-1:1]$. Figure from [2]

rotational and a dilatational order parameter were also defined and measured; finding, however, that these quantities too have very small values (Fig. 3.2).

The rotational order parameter is defined as,

$$R = \frac{1}{N} \left| \sum_i \frac{\boldsymbol{y}_i^{\perp}(t) \times \boldsymbol{v}_i(t)}{|\boldsymbol{y}_i^{\perp}(t) \times \boldsymbol{v}_i(t)|} \cdot \hat{K} \right| \ , \tag{3.1}$$

where $\boldsymbol{y}_i^{\perp}$ is the projection of $\boldsymbol{y}_i(t)$ on the plane orthogonal to the axis of rotation, the cross indicates a vectorial product, and $\hat{K}$ is a unit vector in the direction of the axis of rotation. In (3.1), $\boldsymbol{y}_i^{\perp}(t) \times \boldsymbol{v}_i(t)$ is the angular momentum of midge i with respect to the axis $\hat{K}$. In a perfectly coherent rotation all individuals would have angular momenta parallel to the axis, so that $R = 1$. In a non coherent system, some of the projections of the angular momentum on $\hat{K}$ would be positive and some negative, so $R \sim 0$.

The dilatational order parameter is defined as,

$$\Lambda = \frac{1}{N} \sum_i \frac{[R\,\boldsymbol{y}_i(t)] \cdot [\boldsymbol{y}_i(t+\Delta t) - R\,\boldsymbol{y}_i(t)]}{|R\,\boldsymbol{y}_i(t)|\,|\boldsymbol{y}_i(t+\Delta t) - R\,\boldsymbol{y}_i(t)|} \ . \tag{3.2}$$

$\Lambda \in [-1, 1]$ and it measures the degree of coherent expansion (positive Λ) and contraction (negative Λ) of the swarm. The values of the order parameters considered are in average very small, but their large fluctuations in time are the first hint of a non trivial system.

The values of the global order parameters indicate that swarms are not in an ordered state of any kind. Still, this does not mean that they are non-interacting systems. If we want to understand better this issue we must look at correlations.

Correlation is the most accessible sign of the presence of interaction between the members of a group. The absence of interaction implies the absence of correlation. Conversely, the presence of correlation implies the presence of interaction [10].

The connected correlation function, $C(r)$, measures to what extent the change in behaviour of individual i is correlated to that of j at distance r. Correlation can be measured for different quantities, but in the case of midges, as with birds and other moving animals, the principal quantity of interest is the velocity. The definition of the correlation function is the same given in equation 1.6, that I recall here,

$$C(r) = \frac{\sum_{ij} \boldsymbol{u}_i \cdot \boldsymbol{u}_j \delta(r - r_{ij})}{\sum_{ij} \delta(r - r_{ij})}, \tag{3.3}$$

where $\boldsymbol{u}_i$ is the (dimensionless) velocity fluctuation of midge i, namely the difference between its full velocity and the mean motion of the swarm. In the case of midges, all the possible global modes (Φ, R and Λ) have to be considered to calculate $\boldsymbol{u}_i$, so that is negligible the probability to find global or external effect in the correlation function $C(r)$.

The form of $C(r)$ in natural swarms is non-trivial (Fig 3.3): at short distances there is strong positive correlation, indicating that midges tend to align their velocity to that of their neighbours; then, after some negative correlation at intermediate distances, $C(r)$ relaxes to no correlation for large distances. The value of r_0 where the $C(r)$ crosses zero gives an estimate of the length scale over which the velocity fluctuations are correlated (see section 1.1.3). The average value of this correlation length over all analysed swarms is, $r_0 \sim 0.19$m. This value is about 4 times larger than the nearest neighbours distance, whose average over all swarms is, $r_1 \sim 0.05$m. Previous works noticed the existence of pairing manoeuvres and flight-path coordination between nearest neighbours [36, 35, 11]. This results, however, indicate that midges influence each other's motion far beyond their nearest neighbour (Fig. 3.3), showing that coordination occurs at a truly collective level.

The observable that measures the capability of the system to react to an external stimulus is the susceptibility. It can be defined as the maximum of the space integral of the correlation function.

$$Q(r) = \frac{1}{N} \sum_{i \neq j}^{N} \boldsymbol{u}_i \cdot \boldsymbol{u}_j \; \theta(r - r_{ij}) \; . \tag{3.4}$$

The $Q(r)$ reaches a maximum for $r = r_0$ (Fig. 3.3). This maximum, $\chi \equiv Q(r_0)$, is a measure of the total amount of correlation present in the system. In statistical physics χ is called susceptibility [27, 10] and it is directly related to the collective response of the system to external perturbations.

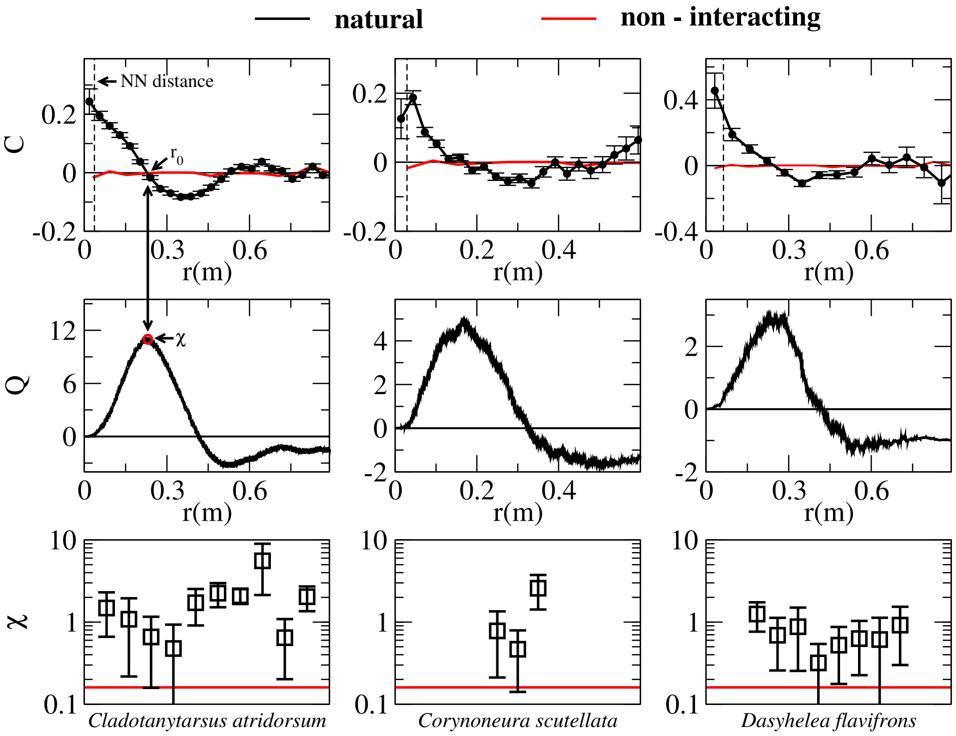

Fig. 3.3: Swarms correlation. Black lines and symbols refer to natural swarms, red lines to simulations of *swarms* of non-interacting particles (NHS). Each column refers to a different midge species. **Top**: Correlation function $C(r)$ as a function of the distance at one instant of time. The dashed vertical line marks the average nearest neighbour distance, r_1, for that swarm. The correlation length, r_0, is the first zero of the correlation function. Red: correlation function in the NHS case. The value of r for the NHS has been rescaled to appear on the same scale as natural distances. Each natural swarm is compared to a NHS with the same number of particles. **Middle:** Cumulative correlation, $Q(r)$. This function reaches a maximum $r = r_0$. The value of the integrated correlation at its maximum, $Q(r_0)$, is the susceptibility χ. **Bottom:** Numerical values of the susceptibility, χ in all analysed swarms. For each swarm the value of χ is a time average over the whole acquisition; error bars are standard deviations. Red: the average susceptibility χ_{NHS} in the non-interacting case. Figure from [2].

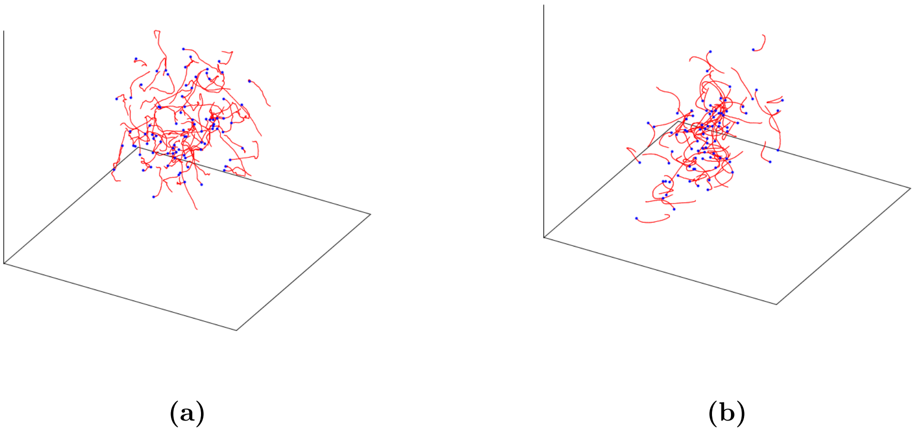
(a) **(b)**

Fig. 3.4: Visual comparison between the noninteracting harmonic (a) swarm and a real swarm (b) trajectories. It is hard to distinguish between the two just looking at the trajectories (or looking at computer animations of real and simulated midges), but the correlation functions are completely different, with the non interacting particles being completely uncorrelated.

3.1.1 Comparison with the noninteracting harmonic swarm

In order to judge how large is χ, we need an effective zero value for it. Following Okubo [35] (but see also [29] and [11]), I implemented and simulated an elementary model of non interacting particles (NHS) performing a random walk in a three-dimensional harmonic potential. The dynamics of each particle is defined by the Langevin equation,

$$m\ddot{\boldsymbol{x}}_i(t) = -\gamma\dot{\boldsymbol{x}}_i(t) - k\boldsymbol{x}_i(t) + \sqrt{\eta\gamma}\boldsymbol{\xi}_i(t) \ , \tag{3.5}$$

where $\boldsymbol{x}_i(t)$ is the position of the i-th particle at time t, m is the mass, γ the friction coefficient, k the harmonic constant and $\boldsymbol{\xi}_i(t)$ is a random vector with zero mean and unit variance, $\langle\xi_i^\alpha(t)\xi_j^\beta(t')\rangle = \delta(t-t')\delta_{i,j}\delta_{\alpha,\beta}$, with $\alpha = x, y, z$. The parameter η tunes the strength of the noise. The equation of motion are integrated with the Euler method [12]. I simulated the NHS in the critically damped regime ($\gamma^2 = 4mk$), which gives the best visual similarity to natural swarms (Fig. 3.4). The number of particles N is set equal to that of the natural swarm we want to compare with. Parameters have been tuned to have a ratio between the distance travelled by a particle in one time step (frame) and the nearest neighbour distance comparable to natural swarms, $\Delta r/r_1 \sim 0.15$: $m = 1, k = 12.75, \gamma = 7.14, \eta = 2.0$.

Despite the visual similarities between the NHS and natural swarms, their correlation functions and susceptibilities are completely different. In the NHS the correlation function $C(r)$ just fluctuates around zero, and the susceptibility is two order of magnitude lower with respect to real swarms. The correlations and susceptibility found in swarms can't belong to a system of non interacting particles just attracted by a marker; there should be some sort of inter individual interaction.

3.1.2 Natural swarms have a metric interaction range

A first hint about the nature of interaction is given by the relation between the value of χ and the nearest neighbour distance $r1$. χ, increases when r_1, decreases (Fig. 3.5). Denser swarms are more correlated than sparser ones. This fact strongly suggests that midges interaction range is metric. If they interact through a metric perceptive apparatus, then the strength of the perception likely decreases with the distance, so that when midges are further apart from each other (larger r_1) the interaction is weaker and the susceptibility χ is lower. In a system ruled by metric interaction we expect all lengths to be measured in units of the perception range, λ. This implies that the natural variable for the susceptibility is the rescaled nearest neighbour distance, r_1/λ. The problem is that we are considering different species, likely to have different metric perception ranges. The simplest hypothesis we can make is that λ is proportional to the insect body length l (which we can measure), so that $\chi = \chi(r_1/l)$. This hypothesis is confirmed by the data: the susceptibility is significantly more correlated to r_1/l (P-value = 0.0004) than to r_1 (P-value = 0.07). The fact that the natural variable is r_1/l is a further indication that the interaction in swarms is based on a metric perception range.

This is very different from what we saw in birds (see section. 1.1.3), where the interaction range is found to be topological: Each bird interact with a fixed number of neighbours, independently of the distances.

The straight forward interpretation for the observed correlations and susceptibility is that midges interaction is based on alignment with individuals within a metric range. This doesn't mean that other type of interaction (e.g. attraction-repulsion) are not present, but a positive velocity correlation on short distance implies that alignment plays a key role.

Since natural swarms have a low polarization, they live in the disordered side of a phase diagram partitioned in ordered and disordered regions, but they also have high correlation, this suggest that they are not too far from the transition point. This hypothesis can be investigated with a comparison between the experimental data and the numerical simulation of a self propelled particles model.

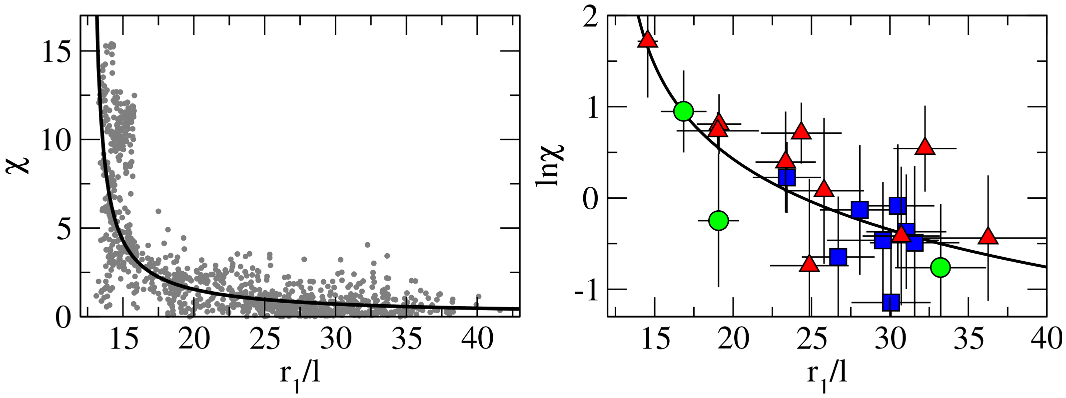

Fig. 3.5: Swarms susceptibility. Left: Susceptibility χ as a function of the rescaled nearest neighbour distance, r_1/l, where l is the body length. Each point represents a single time frame of a swarming event, and all events are reported on the same plot (symbols are the same for all species). The full line is the best fit to equation (3.10). **Right:** Logarithm of the average susceptibility as a function of r_1/l. *Dasyhelea flavifrons* - blue squares; *Corynoneura scutellata* - green circles; *Cladotanytarsus atridorsum* - red triangles. The full line represents the best fit to equation (3.10). Each data point represents the time average over the entire acquisition of one swarming event. Error bars indicate standard deviations. Figure from [2].

3.2 Comparison with Vicsek model

Among the many numerical models of collective behaviour, the original Vicsek model (see section 1.2.1) is the simplest one with all the needed ingredients to make a comparison with the observed swarms.

It is based on alignment interaction rule, the interaction range is metric, and exhibits a density driven phase transition between the ordered and disordered phases.

Since it's known that midges interact also with a landmark I added a central potential to the Vicsek's equations of motion to mimic this feature. equation 1.10 is thus modified as,

$$\boldsymbol{v}_i(t+1) = v_0 \, \mathcal{R}_\eta \left[\Theta \left(\sum_{j \in S_i} \boldsymbol{v}_j(t) - \beta \boldsymbol{r}_i(t) \right) \right] \qquad \beta \geq 0, \tag{3.6}$$

where the term $\beta \boldsymbol{r}_i(t)$ is a force directed toward the origin of the reference frame. The parameter β determines the strength of this force and thus the volume taken by the swarm in free boundary conditions. When β is zero, the original model is recovered.

The update rule of the position remains the same as equation (1.11)

$$\boldsymbol{r}_i(t+1) = \boldsymbol{r}_i(t) + \boldsymbol{v}_i(t+1). \tag{3.7}$$

I studied both variants of the model: the original Viksek's one with periodic boundary conditions, and the central potential one in open boundaries. The two models result qualitatively similar with small differences in the critical exponents that I will mention in the next section.

Both standard Vicsek and central potential models display an ordering transition: at large density, for $x < x_c$ the system is ordered and moves on a straight line in the standard model with periodic boundary conditions, while it forms a group that coherently *orbits* around the potential minimum when the central force is active. Anyway, differently from birds, we are interested in the disordered phase, as midges are disordered. And particularly we want to study the behaviour of the system when it reaches the transition point from the disordered side. The correlation function is nontrivial when x is sufficiently close to x_c (Fig. 3.6), indicating a correlation length higher than the interaction range. I calculated the susceptibility χ, in the same manner as we did for natural

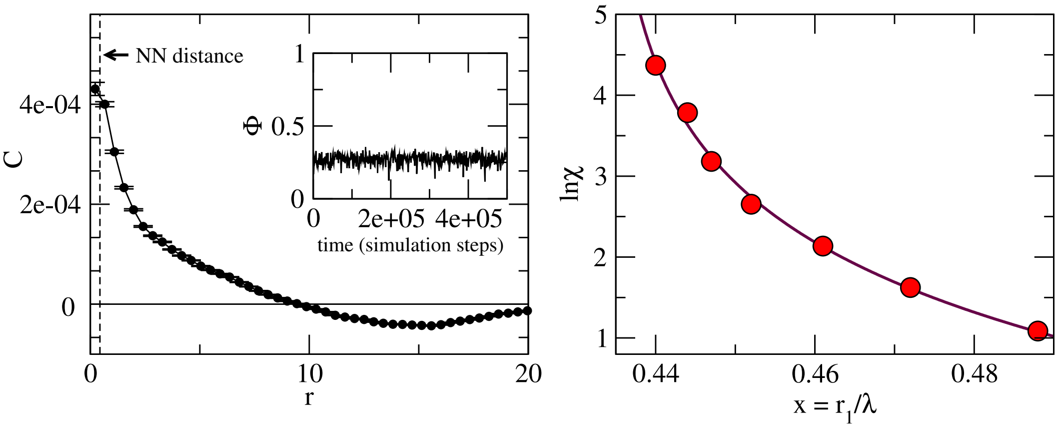

Fig. 3.6: Vicsek model. Three-dimensional Vicsek model in a central potential. **Left:** Correlation function $C(r)$ in the disordered phase, but close to the ordering transition. The dashed line is the nearest neighbour distance. Inset: polarization as a function of time. For this value of x the system is disordered. **Right:** Logarithm of the susceptibility as a function of the rescaled nearest neighbour distance, $x = r_1/\lambda$, where λ is the metric interaction range. Figure from [2].

swarms, in the disordered phase, $x > x_c$ and find a clear increase of χ on lowering x (Fig. 3.6).

The right panels of figures 3.6 and 3.5 are qualitatively consistent one with each other. The natural question is if it's possible to understand something more about swarming midges from a deeper study of the Vicsek model, and if a quantitative comparison is possible. I'll try to address these question in the next section.

3.2.1 Finite size analysis and critical behaviour in the Vicsek model

Given the similarity between real data on midges and the behaviour of the Vicsek model, we decided to use the Vicsek model to understand how the various quantities change approaching the critical point in systems of finite size (which is the case in real swarms).

In the Vicsek model, it's possible to observe a phase transition between the ordered and disordered state, using either noise or density as the control parameter. The nature of the Vicsek's phase transition has been the subject of an intense debate [46, 21, 24, 25, 20] and proved to be first order, but unless N is very large it is indistinguishable from a second order transition (weak first order [10]). To verify the criticality hypothesis on midges swarm, I performed a finite size scaling analysis (FSS) on the Vicsek model, using the rescaled nearest neighbour distance $x = r_1/\lambda$ as a control parameter (being λ the interaction range). This was the first FSS analysis performed for the 3D Vicsek model.

Finite Size scaling has been widely studied in equilibrium systems [38], and more recently proved to hold also in some out of equilibrium ones [41] and in particular in the 2D Vicsek model [46, 6]. In the 3D Vicsek model evidence of FSS are shown in (Fig. 3.8a). The susceptibility χ was calculated as for real data for different system sizes ($N \in [128, 8192]$), varying the control parameter x. Decreasing x (increasing density) from a maximum (minimum) value, we observe that χ has a peak at $x_{max}(N)$. $x_{max}(N)$ is the (size dependent) *critical* value of the control parameter, marking the crossover between the ordered (low x) and disordered (high x) phases. For large system sizes the peak of $\chi(x)$ becomes sharper, and the $x_{max}(N)$ decreases, according to the FSS equation,

$$x_{max}(N) = x_c + N^{-\frac{1}{3\nu}}, \tag{3.8}$$

where ν is the critical exponent of the correlation length ξ. The scaling variable (at fixed noise) is thus, $y = (x - x_c)N^{1/3\nu}$, so that $\chi = N^{\gamma/3\nu} f(y)$ and $\xi = Lg(y)$, where f and g are scaling functions (Fig. 3.8a inset).

An estimate of the values of x_c, ν and γ can be obtained using the scaling relations (Fig. 3.7). We first need an estimate of $\chi_{max}(N)$ and $x_{max}(N)$ corresponding to the peaks of the susceptibility (Fig. 3.7a); then we easily obtain the value of $\gamma/3\nu$ with a linear fit of $\log(\chi) = \gamma/3\nu \log(N)$; and the values ν and x_c fitting $1/3\nu \log(N) = \log(x_{max} - x_c)$ and looking for the value of x_c that gives the lowest reduced chisquare of the fit (Fig. 3.7b).

I obtained $x_c = 0.421 \pm 0.002$, $\gamma = 1.6 \pm 0.1$ and $\nu = 0.75 \pm 0.02$ for the standard Vicsek model; and $x_c = 0.433 \pm 0.002$, $\gamma = 1.5 \pm 0.1$ and $\nu = 0.74 \pm 0.05$ for the central potential variant.

3.2.2 Using Vicsek to understand swarms

My FSS analysis of the Vicsek model gives us a general scenario where we can check how the susceptibility changes with changing the size and the density

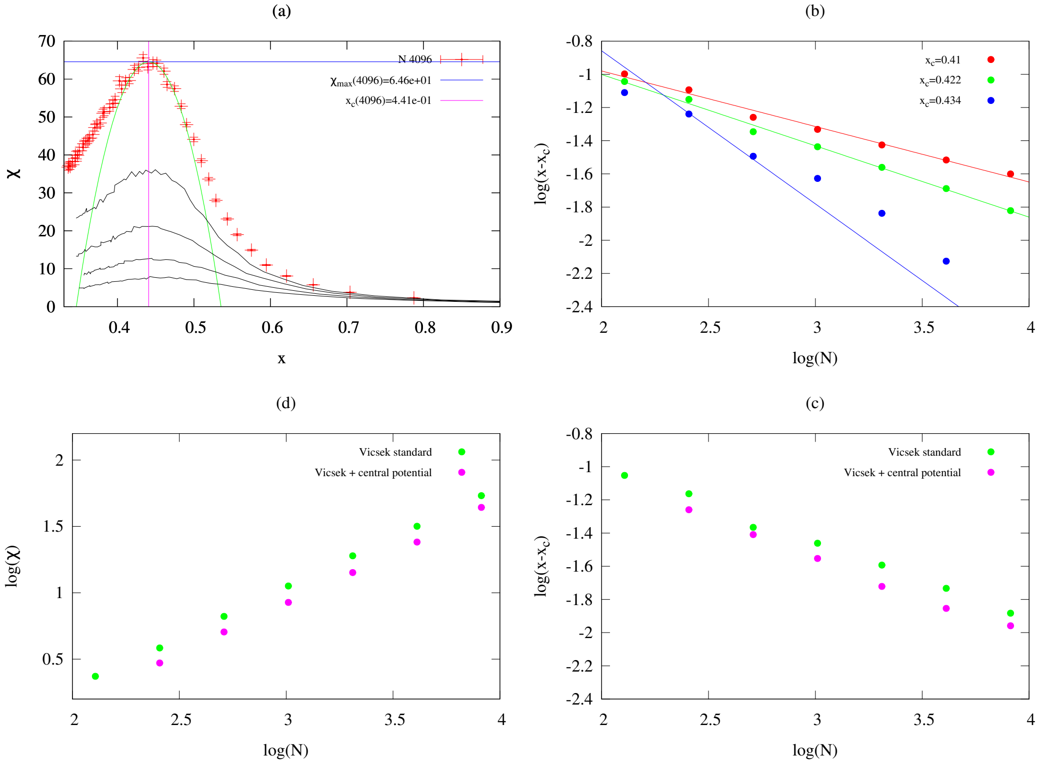

Fig. 3.7: Finite size scaling in the Vicsek model. **(a)** Estimate $\chi_{max}(N)$ and $x_{max}(N)$ by quadratic fit around each peak of $\chi(x, N)$. **(b)** Linear fit of $\log(N) = 3\nu \log(x_{max} - x_c)$ for different values of x_c In the standard model. The optimal x_c (green points) corresponds to the value returns the best linear relation; i.e. that gives the lowest reduced chisquare of a linear fit. **(c)** $Log(\chi)$ vs. $Log(N)$ and **(d)** $\log(x_{max} - x_c)$ vs. $\log(N)$ in the standard Vicsek model and its central potential variant. The linear fit give respectively. $x_c = 0.421 \pm 0.002$, $\gamma/3\nu = 0.756 \pm 0.007$, $1/3\nu = 0.44 \pm 0.02$ and $x_c = 0.433 \pm 0.002$, $\gamma/3\nu = 0.78 \pm 0.05$, $1/3\nu = 0.45 \pm 0.01$

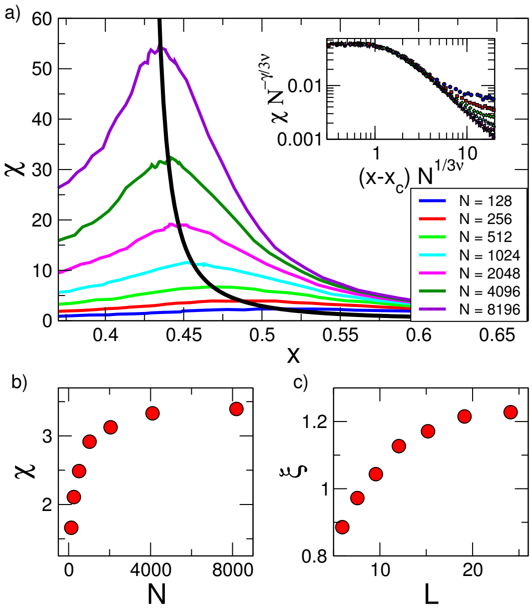

Fig. 3.8: **(a)** Susceptibility χ as a function of the rescaled nearest neighbour distance,$x = r_1/\lambda$ for different swarm sizes N. The maximum of χ occurs at the finite-size critical point, $x_{max}(N)$. This maximum becomes sharper and sharper for increasing N. **Inset:** rescaled susceptibility $\chi N^{-\gamma/\nu}$ vs. scaling variable $xL^{1/\nu}$. The curves nicely rescale one on top of the other. **(b)** Susceptibility as a function of the number of midges N in the swarm. After an initial increase the susceptibility saturates to its bulk finite value. **(c)** Correlation length, ξ, as a function of the linear system size, L. Also the correlation length saturates for large systems. Figure from [5].

of the system. This is an interesting point because we can then compare with what happens in real swarms, where indeed size and density change from swarm to swarm.

In figures 3.8b and 3.8c we observe that at a fixed value of $x > x_c$ both the susceptibility and the correlation length grow when N is increased, until they saturate to the (finite) bulk value. This is *not* what we observe in real swarms, where the susceptibility scales with N and correlation length with L up to largest observed sizes figures 3.9a and 3.9b.

In fact, there is no reason why natural swarms should maintain their control parameter x fixed. While it is surely true that there could eventually be a saturation of χ and ξ for larger (unobserved) swarms, the actual *state-of-the-art* data shows no hint of such saturation. This suggest that, in natural swarms, when N is increased then x is decreased, following the peak of the susceptibility, and poising the system near criticality.

If N and x are tuned to keep constant the scaling variable $y = (x - x_c)N^{1/3\nu}$, then the following relations must hold,

$$\chi \sim N^{\frac{\gamma}{3\nu}}, \tag{3.9a}$$

$$\xi \sim L \tag{3.9b}$$

$$x \sim x_c + N^{-\frac{1}{3\nu}}. \tag{3.9c}$$

As I show in figure 3.9(a, b and c) the experimental data are compatible with these equation, particularly in figure 3.9c the correlation between the control parameter and system size is evident. If the system is such that the parameters N and x are naturally adjusted to stay near the critical region (3.9c is satisfied), then the susceptibility χ must depend on x as (Fig. 3.9d),

$$\chi \sim \frac{1}{(x - x_c)^{\gamma}}. \tag{3.10}$$

In the lower panels of (Fig. 3.9), results obtained with the Vicsek model are shown for comparison. In this case N and x were manually set to keep constant $y = (x - x_c)N^{1/3\nu}$.

We can ask if there is some other quantitative conclusion we can catch about the midges swarm from the comparison with the Vicsek model. If a Vicsek-like ordering transition exist, we can use equation (3.10) to fit the swarms data for χ (Fig. 3.5). As I already mentioned, we do not know the value of the metric perception range, λ, in swarms. Therefore, we must use as scaling variable

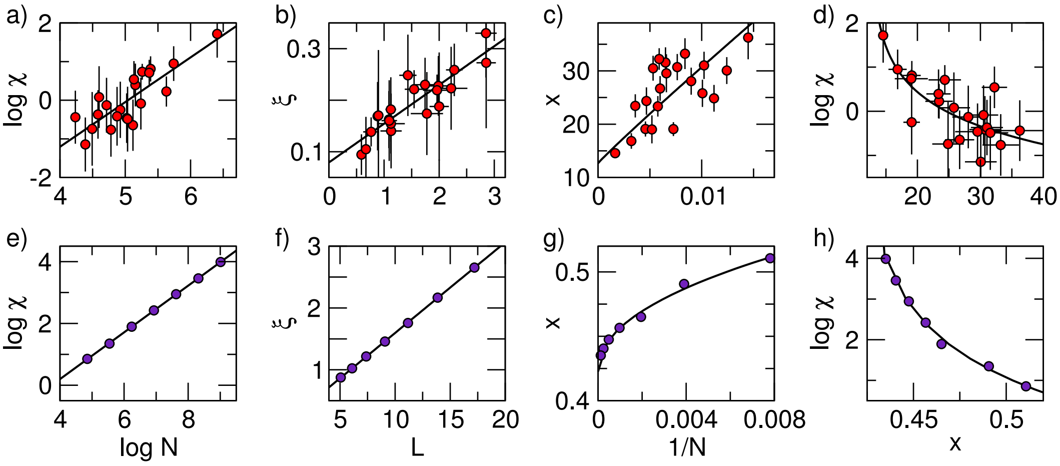

Fig. 3.9: Scaling behaviour in natural swarms. (a) Susceptibility as a function of the number of midges N in the swarm.There is no evident sign of saturation, suggesting that swarms are in a scaling regime. **(b)** Correlation length, ξ, as a function of the linear system size, L. Also the correlation length, consistently with the susceptibility, shows no saturation for large systems. **(c)** Control parameter $x = r_1/l$ as a function of sister size N: a clear correlation between these two quantities is present in the data indicating that the system self-adjusts density and size. **(d)** Susceptibility as a function of the control parameter $x = r_1/l$: data are consistent with a power law dependence, as predicted by finite-size scaling theory in the near-critical region. Lower panels (e,f,g,h): same quantities as in upper panels for the Vicsek model in the critical region. Figure from [5].

r_1/l, where l is the body length. From the fit we obtain $(r_1/l)_c = 11.0 \pm 2.0$ and $\gamma = 1.0 \pm 0.2$.

If we make the hypothesis that the growth of the susceptibility is a universal mechanism ruled by the ordering phase transition, we have that the critical nearest neighbour distance $(r_1)_c$ in its natural units must be the same in Vicsek as in natural swarms. We conclude that, $0.43\,\lambda \sim 11\,l$, that is (including errors), $\lambda \sim 21\,l - 26\,l$. The body length of the species we consider is in the range, $l \sim$ 1.2mm–2.4mm. This implies a perception range of a few centimetres, $\lambda \sim 2.5 - 6.0$cm.

Even if probably reasonable This estimate of the midges interaction range has to be taken with maximum cautiousness, because the critical value of x

in the Vicsek model depends by the chosen parameters, that remains quite arbitrary even if I tried to tune the parameters to obtain a maximum value of the (dimensionless) susceptibility $\chi(N)$ comparable to the one observed in swarms (at same values of N). Moreover the values of $(r_1/l)_c$ and γ, obtained for the real swarms, have a large error due to the scatter of the data, the non linear nature of the fit, and the relatively small range of the system sizes.

What is much more solid is the criticality of the system. Being near the critical point of a phase transition has a clear advantage from the biological point of view. At the critical point the system has the higher possible response to a perturbation as it is particularly clear looking at the Vicsek's $\chi(x)$ in figure 3.8. The information can propagate over long distances. Away from criticality, a signal visible to one midge can influence just a handful of near neighbours; at criticality, the same signal can spread to influence the behaviour of the entire swarm.

There are two possible interpretations of this result. The first is that given a size N the control parameter x is tuned to maximize correlations. This would mean that individuals in the swarm are able to *measure* the size of the system and modify their behaviour accordingly to it. It seam more plausible the opposite, for a given value of x the system grows by aggregation of new individuals until the optimal value of $N_{max}(x)$ is reached. If the swarm grows so that $N > N_{max}(x)$, then it lose correlation since the ratio ξ/L decreases, leading to statistically independent clusters, and deteriorating the collective response.

Conclusions

The numerical simulations of physical systems are a widely used instrument in scientific investigation. When the laws governing the system are known they allow to perform synthetic *experiments* and study the system's behaviour; while when the object of study in unknown they help to understand how likely an intuition can be. This is particularly true in statistical mechanics where linking the behaviour of the single particles with the behaviour of the whole system can be extremely difficult.

In the field of collective animal behaviour the numerical models played an unusual role, they where the main source of information before the availability of experimental results.

Here I presented new results obtained from the study of numerical models that are strongly connected with the experiments and the theories based upon them.

The analysis of the spatial anisotropy of the neighbours distribution of a bird revealed that the interaction range of starlings is topological rather than metric: each bird interacts with its first $6 \sim 7$ neighbours independently from their metric distances. This was also confirmed by the maximum entropy theory through parameters inference. In section 1.2.3 I linked this experimental finding with a plausible biological outcome: to grant the stability of the flock. This is matter of life or death for the birds; being cohesive is in fact their best defensive strategy against predators. In addition finding an optimal interaction strategy is interesting in other fields; for example in robotics there is a growing interest in the idea that many autonomous simple robots can collectively perform complex tasks. I described and studied a novel topological model, showing that the topological interaction outperforms the metric one in granting the cohesion of the flock. I showed that a topological interaction, being invariant with respect to local density fluctuations, makes the flock less susceptible to fragmentation due to noise or external obstacles. The number of interacting neighbours needed for each bird to ensure a cohesive flock is significantly smaller if the interaction range is topological than if it is metric, saving the (supposedly) limited cognitive capacities of a single bird.

In section 1.3 I summarized a powerful statistical inference method: the maximum entropy method. It consists in finding the less structured probability distribution compatible with the experimental findings, and inferring the distribution's parameter. The application of the maximum entropy method to the experimental data confirmed the topological nature of the interaction, providing an inferred interaction range $n_c \sim 21$; three times bigger than the previously discussed one. The maximum entropy theory was developed to study equilibrium systems, while bird flocks are intrinsically out-of-equilibrium, I therefore used numerical simulations to test the method on active off-equilibrium systems. I applied the inference equations to the synthetic data from a self-propelled particle model and showed that they provide an excellent estimate of the model's parameters, biased only by a proportionality factor. Interestingly, rescaling the value of n_c of the birds by this proportionality factor we retrieve the same interaction range previously obtained with a completely independent method.

Historically all models of collective behaviour are based on assumptions. One example over all is the Vicsek model; the birds in a flock are aligned, so alignment interaction is the key assumption of the model. Although they can be reasonable, assumptions need to be experimentally verified, and, again in the Vicsek model, the assumption that interactions are based on a metric range was instead proved wrong (in the case of bird flocks). In section 1.3.4 I described a different approach to model definition consisting in deriving it from data. I discussed an experimental result: the scale free correlation of speed fluctuations; and a theoretical result: the probability distribution consistent with the experiment. The new model is derived from a mechanistic interpretation of the theoretical probability distribution limiting assumptions to the lowest possible level (ideally null). This model reproduces the experimentally measured long-range correlation of the speed of the birds; and it shows that, in order to do it, the system has to be critical, i.e. a control parameter has to be near to its critical value. Additionally I showed that a theory that provides only static (instantaneous) probability distributions remains valid also when the full dynamical features of the system are taken in account.

The second chapter concerns one of the most important issues in collective behaviour: how information propagates through the system. Even being out-of-equilibrium, a flock of birds flying on a straight line can be considered in a stationary state, thus is well described by stationary probability distributions.

Obviously bird flocks do not only flight on a straight line, but also change their direction; they do it collectively and almost instantaneously. Experiments revealed us that the turning information travels across the flock at a constant rate with very low attenuation. This constant rate information transfer can not be described by the classic theory due to the missing of two crucial ingredients: a conservation law associated with the rotational symmetry, and a term of behavioural inertia. In section 2.2.1 I introduced a new model that accounts for these two ingredients; I described how I implemented numerically this new model and I provided a deep study of the role of the model parameters in the information transfer process. I showed that the models exhibits two different regimes, propagating and not-propagating directional information, depending on the damping parameter, and being in the strongly overdamped regime equivalent to the Vicsek model. I also showed that the theoretically predicted dependence of the speed of propagation of the signal from the parameters, and its non-trivial relation with the alignment are correctly reproduced by the model.

Finally in the third chapter I considered a system completely different from bird flocks: the midge swarms. The collective nature of the behaviour of midge swarms is not immediately evident as it is in flocks; they seem, and indeed measured to be, disordered. I examined how order is not the key feature of collective behaviour, while correlation is. Experiments revealed that midge swarm are strongly correlated; that their interaction is based on alignment and that their interaction range is metric. I showed that the experimental correlations can be reproduced by the Vicsek model, in its original definition with periodic boundary conditions and in a variant where a global central force is applied to all the particles. I showed that such correlations are well reproduced when the model lies in a particular region of the phase diagram: the critical region. I reported the first finite size scaling analysis of the three-dimensional Vicsek model and compared the scaling variables with the ones of real swarms, supporting the criticality hypothesis. The analysis performed on both real and synthetic data revealed that *being critical* in a finite size system has a slightly different meaning with respect to what we are used to think in the thermodynamic limit; the latter has a precise value of the control parameter that define the critical point, while in a finite size system the *pseudo-critical* value of the control parameter depends in a not trivial way by the system size (i.e. the maximum of the susceptibility). Finally I proposed a parameter fitting method to infer the interaction range of midges.

As conclusion I would recall the striking title of a paper from Thierry Mora and William Bialek: *Are biological systems poised at criticality?* [31]. There is not an universal answer to this question, but the evidences of criticality in two very different systems as flocks and swarms are intriguing. We don't know if the scale free correlation measured in experiments are so just because the considered system sizes are too small and so we missed a saturation of the correlation length. In this case however we can still say that the systems studied are *near* the critical point, thus we can think that evolution favoured this near criticality to maximize the efficiency of the system. On the other side we can speculate that if evolution leads to efficiency then, for an arbitrary size, a collective biological system must be as near to criticality as needed to obtain long range correlations, and thus collective responses. This is likely to be a general law.

Bibliography

[1] Daniel J. Amit and Victor Martin-Mayor: *Field Theory, The Renormalization Group and Critical Phenomena.* World Scientific Publishing Company, 2005, ISBN 978-9812561190.

[2] Alessandro Attanasi, Cavagna Andrea, Del Castello Lorenzo, Giardina Irene, Melillo Stefania, Parisi Leonardo, Pohl Oliver, Rossaro Bruno, Shen Edward, Silvestri Edmondo, and Viale Massimiliano: *Collective Behaviour without Collective Order in Wild Swarms of Midges.* PLoS Comput Biol, 10(7):e1003697, July 2014.

[3] Alessandro Attanasi, Andrea Cavagna, Lorenzo Del Castello, Irene Giardina, Tomas S. Grigera, Asja Jelic, Stefania Melillo, Leonardo Parisi, Oliver Pohl, Edward Shen, and Massimiliano Viale: *Information transfer and behavioural inertia in starling flocks.* Nat Phys, 10(9):691–696, September 2014.

[4] Alessandro Attanasi, Andrea Cavagna, Lorenzo Del Castello, Irene Giardina, Asja Jelic, Stefania Melillo, Leonardo Parisi, Fabio Pellacini, Edward Shen, Edmondo Silvestri, and others: *Tracking in three dimensions via recursive multi-path branching.* preprint arXiv:1305.1495, 2013.

[5] Alessandro Attanasi, Andrea Cavagna, Lorenzo Del Castello, Irene Giardina, Stefania Melillo, Leonardo Parisi, Oliver Pohl, Bruno Rossaro, Edward Shen, Edmondo Silvestri, and Massimiliano Viale: *Finite-size scaling as a way to probe near-criticality in natural swarms.* Phys. Rev. Lett., 113:238102, Dec 2014.

[6] Gabriel Baglietto and Ezequiel V. Albano: *Finite-size scaling analysis and dynamic study of the critical behavior of a model for the collective displacement of self-driven individuals.* Physical Review E, 78(2):021125, 2008.

[7] Michele Ballerini, Nicola Cabibbo, Raphael Candelier, Andrea Cavagna, Evaristo Cisbani, Irene Giardina, Vivien Lecomte, Alberto Orlandi, Giorgio Parisi, Andrea Procaccini, and others: *Interaction ruling animal collective behavior depends on topological rather than metric distance: Evidence from a field study.* Proceedings of the National Academy of Sciences, 105(4):1232–1237, 2008.

[8] William Bialek, Andrea Cavagna, Irene Giardina, Thierry Mora, Oliver Pohl, Edmondo Silvestri, Massimiliano Viale, and Aleksandra M. Walczak: *Social interactions dominate speed control in poising natural flocks near criticality.* Proceedings of the National Academy of Sciences, 111(20):7212–7217, 2014.

[9] William Bialek, Andrea Cavagna, Irene Giardina, Thierry Mora, Edmondo Silvestri, Massimiliano Viale, and Aleksandra M. Walczak: *Statistical mechanics for natural flocks of birds.* Proceedings of the National Academy of Sciences, 109(13):4786–4791, 2012.

[10] James J. Binney, N. J. Dowrick, A. J. Fisher, and M. Newman: *The theory of critical phenomena: an introduction to the renormalization group.* Oxford University Press, Inc., 1992.

[11] Sachit Butail, Nicholas C. Manoukis, Moussa Diallo, José MC Ribeiro, and Derek A. Paley: *The dance of male Anopheles gambiae in wild mating swarms.* Journal of medical entomology, 50(3):552–559, 2013.

[12] John C. Butcher: *Numerical methods for ordinary differential equations.* John Wiley & Sons, 2008.

[13] Marcelo Camperi, Andrea Cavagna, Irene Giardina, Giorgio Parisi, and Edmondo Silvestri: *Spatially balanced topological interaction grants optimal cohesion in flocking models.* Interface Focus, 2(6):715–725, 2012.

[14] A. Cavagna, I. Giardina, T. S. Grigera, A. Jelic, D. Levine, S. Ramaswamy, and M. Viale: *Silent Flocks.* preprint arXiv:1410.2868, October 2014.

[15] Andrea Cavagna, Alessio Cimarelli, Irene Giardina, Alberto Orlandi, Giorgio Parisi, Andrea Procaccini, Raffaele Santagati, and Fabio Ste-

fanini: *New statistical tools for analyzing the structure of animal groups.* Mathematical biosciences, 214(1):32–37, 2008.

[16] Andrea Cavagna, Alessio Cimarelli, Irene Giardina, Giorgio Parisi, Raffaele Santagati, Fabio Stefanini, and Massimiliano Viale: *Scale-free correlations in starling flocks.* Proceedings of the National Academy of Sciences, 107(26):11865–11870, 2010.

[17] Andrea Cavagna, Lorenzo Del Castello, Irene Giardina, Tomas Grigera, Asja Jelic, Stefania Melillo, Thierry Mora, Leonardo Parisi, Edmondo Silvestri, Massimiliano Viale, and AleksandraM. Walczak: *Flocking and turning: a new model for self-organized collective motion.* Journal of Statistical Physics, pages 1–27, 2014.

[18] Andrea Cavagna, Irene Giardina, Alberto Orlandi, Giorgio Parisi, and Andrea Procaccini: *The STARFLAG handbook on collective animal behaviour: 2. Three-dimensional analysis.* Animal Behaviour, 76(1):237–248, 2008.

[19] Andrea Cavagna, Irene Giardina, Alberto Orlandi, Giorgio Parisi, Andrea Procaccini, Massimiliano Viale, and Vladimir Zdravkovic: *The STARFLAG handbook on collective animal behaviour: 1. Empirical methods.* Animal Behaviour, 76(1):217–236, 2008.

[20] Hugues Chaté, Francesco Ginelli, Guillaume Grégoire, and Franck Raynaud: *Collective motion of self-propelled particles interacting without cohesion.* Physical Review E, 77(4):046113, 2008.

[21] András Czirók, Mária Vicsek, and Tamás Vicsek: *Collective motion of organisms in three dimensions.* Physica A: Statistical Mechanics and its Applications, 264(1):299–304, 1999.

[22] J. A. Downes: *The swarming and mating flight of Diptera.* Annual review of entomology, 14(1):271–298, 1969.

[23] Vincent Garcia, Eric Debreuve, and Michel Barlaud: *Fast k nearest neighbor search using GPU.* In *Computer Vision and Pattern Recognition Workshops, 2008. CVPRW'08. IEEE Computer Society Conference on*, pages 1–6. IEEE, 2008.

[24] Balázs Gönci, Máté Nagy, and Tamás Vicsek: *Phase transition in the scalar noise model of collective motion in three dimensions.* The European Physical Journal-Special Topics, 157(1):53–59, 2008.

[25] Guillaume Grégoire and Hugues Chaté: *Onset of collective and cohesive motion.* Physical review letters, 92(2):025702, 2004.

[26] Guillaume Grégoire, Hugues Chaté, and Yuhai Tu: *Moving and staying together without a leader.* Physica D: Nonlinear Phenomena, 181(3):157–170, 2003.

[27] K. Huang: *Slatistical Mechanics.* Wiley, Ne∼ York, 1963.

[28] Edwin T. Jaynes: *Information theory and statistical mechanics.* Physical review, 106(4):620, 1957.

[29] Douglas H. Kelley and Nicholas T. Ouellette: *Emergent dynamics of laboratory insect swarms.* Scientific reports, 3, 2013.

[30] Timothy R. Lezon, Jayanth R. Banavar, Marek Cieplak, Amos Maritan, and Nina V. Fedoroff: *Using the principle of entropy maximization to infer genetic interaction networks from gene expression patterns.* Proceedings of the National Academy of Sciences, 103(50):19033–19038, 2006.

[31] Thierry Mora and William Bialek: *Are biological systems poised at criticality?* Journal of Statistical Physics, 144(2):268–302, 2011.

[32] Thierry Mora, Aleksandra M. Walczak, William Bialek, and Curtis G. Callan: *Maximum entropy models for antibody diversity.* Proceedings of the National Academy of Sciences, 107(12):5405–5410, 2010.

[33] G. M. Morton: *A computer oriented geodetic data base and a new technique in file sequencing.* In *IBM Germany Scientific Symposium Series.* IBM Ltd., 1966.

[34] Atsuyuki Okabe, Barry Boots, Kokichi Sugihara, and Sung Nok Chiu: *Spatial tessellations: concepts and applications of Voronoi diagrams*, volume 501. John Wiley & Sons, 2009.

[35] Akira Okubo: *Dynamical aspects of animal grouping: swarms, schools, flocks, and herds.* Advances in biophysics, 22:1–94, 1986.

[36] Akira Okubo and H. C. Chiang: *An analysis of the kinematics of swarming ofAnarete Pritchardi Kim (Diptera: Cecidomyiidae).* Researches on Population Ecology, 16(1):1–42, 1974.

[37] Jack A. Orenstein: *Spatial query processing in an object-oriented database system.* In *Proceedings of the 1986 ACM SIGMOD International Conference on Management of Data*, SIGMOD '86, pages 326–336, New York, NY, USA, 1986. ACM.

[38] Finite Size Scaling: *Numerical Simulation of Statistical Systems, edited by V. Privman.* World Scientific, Singapore, 1990.

[39] Elad Schneidman, Michael J. Berry, Ronen Segev, and William Bialek: *Weak pairwise correlations imply strongly correlated network states in a neural population.* Nature, 440(7087):1007–1012, 2006.

[40] Claude Elwood Shannon: *A mathematical theory of communication.* ACM SIGMOBILE Mobile Computing and Communications Review, 5(1):3–55, 2001.

[41] S. W. Sides, P. A. Rikvold, and M. A. Novotny: *Kinetic Ising model in an oscillating field: Finite-size scaling at the dynamic phase transition.* Physical review letters, 81(4):834, 1998.

[42] Aonan Tang, David Jackson, Jon Hobbs, Wei Chen, Jodi L. Smith, Hema Patel, Anita Prieto, Dumitru Petrusca, Matthew I. Grivich, Alexander Sher, and others: *A maximum entropy model applied to spatial and temporal correlations from cortical networks in vitro.* The Journal of Neuroscience, 28(2):505–518, 2008.

[43] G. Tkačik: *Information flow in biological networks.* PhD thesis, Princeton University, 2007.

[44] Gašper Tkačik, Olivier Marre, Thierry Mora, Dario Amodei, Michael J. Berry II, and William Bialek: *The simplest maximum entropy model for collective behavior in a neural network.* Journal of Statistical Mechanics: Theory and Experiment, 2013(03):P03011, 2013.

[45] John Toner and Yuhai Tu: *Flocks, herds, and schools: A quantitative theory of flocking.* Physical review E, 58(4):4828, 1998.

[46] Tamás Vicsek, András Czirók, Eshel Ben-Jacob, Inon Cohen, and Ofer Shochet: *Novel type of phase transition in a system of self-driven particles.* Physical review letters, 75(6):1226, 1995.

List of Publications

[1] William Bialek, Andrea Cavagna, Irene Giardina, Thierry Mora, Edmondo Silvestri, Massimiliano Viale, and Aleksandra M. Walczak: Statistical mechanics for natural flocks of birds. Proceedings of the National Academy of Sciences, 109(13):4786–4791, 2012.

[2] Marcelo Camperi, Andrea Cavagna, Irene Giardina, Giorgio Parisi, and Edmondo Silvestri: Spatially balanced topological interaction grants optimal cohesion in flocking models. Interface Focus, 2(6):715–725, 2012.

[3] Alessandro Attanasi, Andrea Cavagna, Lorenzo Del Castello, Irene Giardina, Asja Jelic, Stefania Melillo, Leonardo Parisi, Fabio Pellacini, Edward Shen, Edmondo Silvestri, and others: Tracking in three dimensions via recursive multi-path branching. preprint arXiv:1305.1495, 2013.

[4] William Bialek, Andrea Cavagna, Irene Giardina, Thierry Mora, Oliver Pohl, Edmondo Silvestri, Massimiliano Viale, and Aleksandra M. Walczak: Social interactions dominate speed control in poising natural flocks near criticality. Proceedings of the National Academy of Sciences, 111(20):7212–7217, 2014.

[5] Alessandro Attanasi, Cavagna Andrea, Del Castello Lorenzo, Giardina Irene, Melillo Stefania, Parisi Leonardo, Pohl Oliver, Rossaro Bruno, Shen Edward, Silvestri Edmondo, and Viale Massimiliano: Collective Behaviour without Collective Order in Wild Swarms of Midges. PLoS Comput Biol, 10(7):e1003697, July 2014.

[6] Andrea Cavagna, Lorenzo Del Castello, Irene Giardina, Tomas Grigera, Asja Jelic, Stefania Melillo, Thierry Mora, Leonardo Parisi, Edmondo Silvestri, Massimiliano Viale, and AleksandraM. Walczak: Flocking and turning: a new model for self-organized collective motion. Journal of Statistical Physics, pages 1–27, 2014.

[7] Alessandro Attanasi, Andrea Cavagna, Lorenzo Del Castello, Irene Giardina, Stefania Melillo, Leonardo Parisi, Oliver Pohl, Bruno Rossaro, Edward Shen, Edmondo Silvestri, and Massimiliano Viale: Finite-size scaling as a way to probe near-criticality in natural swarms. Phys. Rev. Lett., 113:238102, Dec 2014.